PASSIVE THERMAL MANAGEMENT OF DISTRIBUTION GRID ASSETS

A Thesis
Presented to
The Academic Faculty

by

Danielle Lauren Hesse

In Partial Fulfillment
of the Requirements for the Degree
Master of Science in the
G.W. Woodruff School of Mechanical Engineering

Georgia Institute of Technology
December 2015

PASSIVE THERMAL MANAGEMENT OF DISTRIBUTION GRID ASSETS

Approved by:

Dr. J. Rhett Mayor, Advisor
G. W. Woodruff School of Mechanical Engineering
Georgia Institute of Technology

Dr. S. Mostafa Ghiaasiaan
G. W. Woodruff School of Mechanical Engineering
Georgia Institute of Technology

Dr. Sheldon Jeter
G. W. Woodruff School of Mechanical Engineering
Georgia Institute of Technology

Date Approved: 07/28/2015

ACKNOWLEDGEMENTS

I would like to thank my committee members, Dr. Jeter and Dr. Ghiaasiaan for their time and consideration in evaluating this work. I greatly appreciate their willingness to provide feedback on this work.

I would also like to acknowledge my lab mates, Noris Gallandat and Nishant Srinivasan for the free discussions and exchanges that have helped me overcome challenging obstacles as well as help me become a better collaborator and engineer. I would also like to thank Dr. Semidey for his guidance and support throughout this process. I would like to thank Benjamin Loeffler for his insight into the work and assistance in this project.

I must also thank Dr. Mayor for his efforts and guidance as an advisor. He constantly challenged my capabilities and without a doubt has molded me into the engineer I am today.

I would like to thank Varentec who funded this project and made the work possible. I would also like to thank NEETRAC and Frank Lambert for their testing facilities and cooperation throughout the experimental phase of this project.

Lastly I would like to thank my family and friends as they supported my efforts throughout this journey.

TABLE OF CONTENTS

LIST OF TABLES

LIST OF FIGURES

SUMMARY

This thesis presents a comprehensive study into the passive thermal management of high-voltage power electronics converters for use in augmented grid assets capable of performing power routing on the electricity grid. The work has focused on the thermal transport of single-phase closed thermosiphon systems incorporating a secondary parallel flow path for cooling an additional, typically smaller, thermal load associated with the power electronics converters. Dual-loop thermosiphon passive thermal management systems were incorporated into a grounded compact dynamic phase angle regulator (GCD-PAR) that aimed to facilitate power routing and reduce line losses on the power grid. The power router utilizes power electronics that reject heat to a planar area, or cold plate, which must be cooled by an entirely passive system to comply with the minimum 30 year mean time between failures (MTBF) consistent with grid reliability requirements. This design includes a secondary-loop cooling path that utilizes the cooling oil already present in the transformer to also cool the power router. An analytical multi-physics thermosiphon model is developed that couples existing fluid dynamic and heat transfer correlations to create a description of the steady state operation of a specific cylindrical 50 kVA transformer augmented with a thermosiphon. The model is validated experimentally and found to solve for steady state baseplate temperatures under maximum load within 2°C in 0.1 seconds. The model is then modified for a specific rectilinear 1 MVA transformer augmented with three thermosiphons. The 1 MVA model is validated experimentally and found to solve for steady state baseplate temperatures under maximum load within 4 °C in 0.2 seconds. The analytical model proves to be accurate and solve quickly with various geometric configurations and thermal loads.

CHAPTER 1

INTRODUCTION

1.1 Smart and controllable grid

The continuous increase of electrical demand along with the increasing level of penetration of renewable energy has increased the need for a smart, dynamically controlled grid. In 2012 alone, the U.S lost over $26 billion to transmission losses, at the average retail price of electricity of $0.1/kW-hr. This totals 263 million MW-hrs and is 8.7% of the total power generated in the United States [1]. Power flow control allows for improving reliability, reducing congestion to minimize line losses and reducing service interruptions by isolating faults. Additional power from renewable resources is continuing to increase, 12.6% from 2011 to 2012 [1]. These renewable resources depend on variables such as wind speed and solar insolation, which are not continuous or reliable. In order to incorporate renewable energy sources, as depicted in Figure 1, the grid has to be improved to handle the asymmetric stresses caused by the variability of these resources [2]. Efficient power routing also enables the renewable energy to be transferred from where it is generated to major load centers, which are generally not close to the point of generation. Augmenting existing grid level transformers with high power solid state electronic converters has the potential to create a smart and controllable grid allowing reliable integration of renewable resources while also decreasing the amount of loss due to transmission.

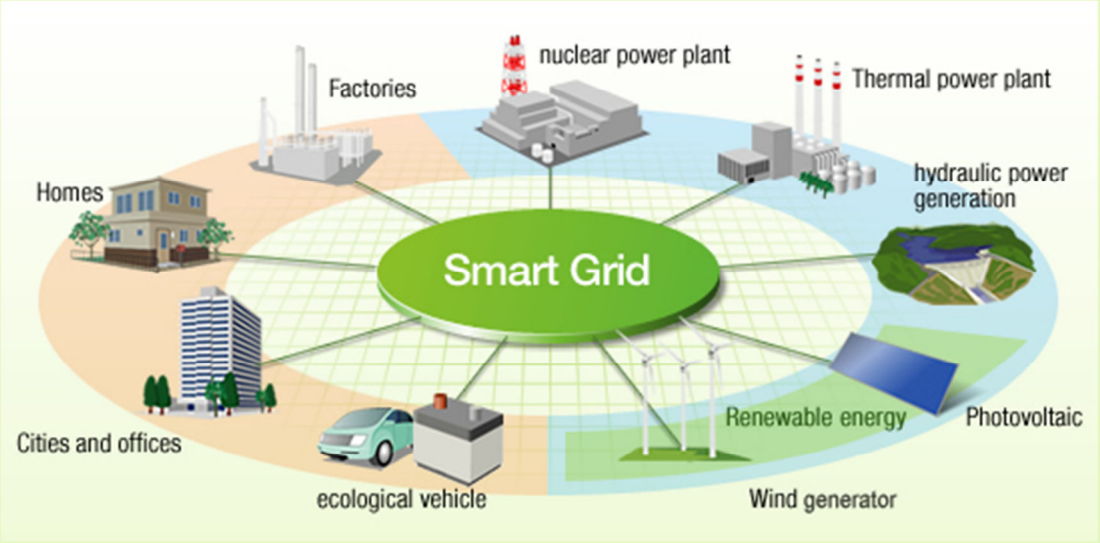

Figure 1. Smart Grid shown incorporating renewable resources [3]

1.2 Power electronics for power routing

Over the last two decades a number of transmission system devices have been proposed for power flow control. Some of the options include, unified power flow controllers and Back to Back HVDC links. These, however, are costly and may not be needed to provide the level of control desired in the grid. Other options include Controllable Network Transformers and compact dynamic phase angle regulators (CD-PAR). The CD-PAR augments the existing grid level transformers with high power solid state electronic converters. These options require their electronics to be floating at the line voltage which increases isolation concerns and can increase complexity and cost. A new technology exits, which utilizes the CD-PAR technology with changes to the transformer topology to make the electronics operate close to ground potential. The "grounded" CD-PAR (GCD-PAR) integrates a fractionally-rated transformer with a converter comprised of AC switches and LC filters to dynamically control grid assets to create a Power Converter Augmented Transformer (PCAT). The GCD-PAR also

preserves system reliability by incorporating a ‘fail-normal’ switch which bypasses the converter under fault conditions. This technology has the potential to create a smart and controllable grid at a low cost by augmenting the existing distribution grid assets.

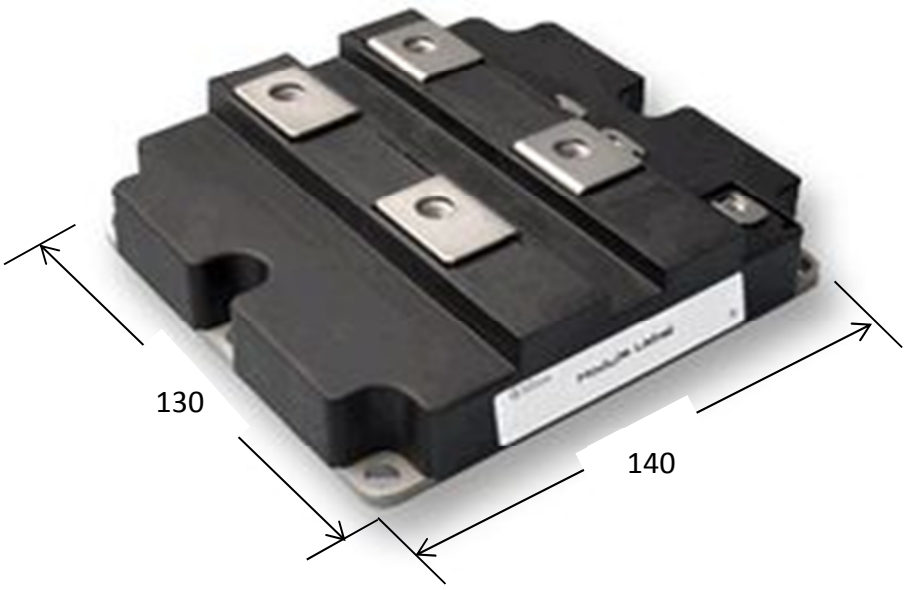

Figure 2. Infineon IGBT module used in the GCD-PAR (dimensions in mm)

The power converters used in the GCD-PAR, like many other high power density technologies, are thermally limited. Progression in the power density of these solid state power converter technologies will likely benefit more from improving the thermal management techniques for the device than from improving the device efficiency. Improved thermal management will allow the existing devices to be pushed harder without any improvements in the loss levels or device efficiency. It is well known that with reduction in chip operating temperature, the reliability of the chip increases exponentially. The success of the GCD-PAR design is largely dependent on a thermal

management system that will keep the converters above the reliability requirements for grid implementation. The IGBT module used for the GCD-PAR, depicted in Figure 2, has a maximum junction temperature of 150°C under the IGBT and 125 °C under the diode and is expected to dissipate 300 W of loss as heat, resulting in heat fluxes close to 2.5 W/cm^2 [4]. The power converter, as depicted in Figure 3, is an AC chopper circuit, implemented through two IGBTs connected in common-emitter and common-collector configurations.

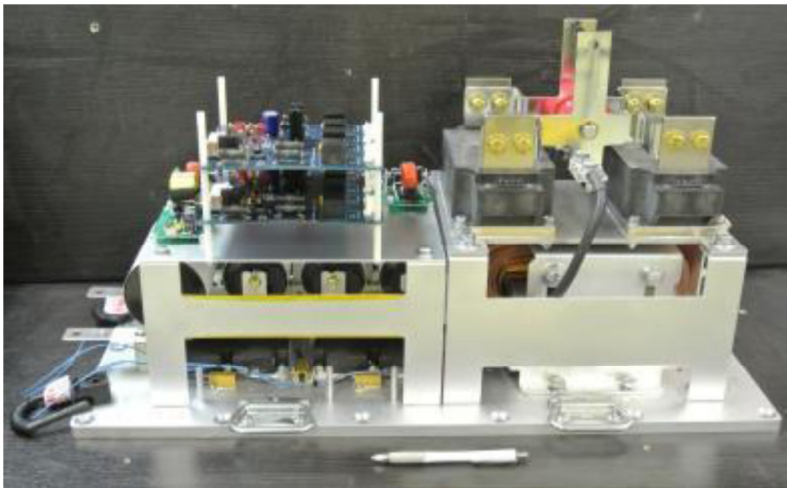

Figure 3. Picture of the power converter on a cold plate [5]

The power converter also contains an inductor expected to dissipate 100 W of loss. Conservatively assuming that all losses are dissipated into the cold plate, 700 W will need to be rejected by the cold plate. This system is also required to operate in ambient conditions up to 40°C.

1.3 Thermal management for grid assets

The GCD-PAR system is required to have a minimum of a 30 year mean time between failures (MTBF) to be incorporated into the electrical grid. Active cooling

systems would meet the necessary cooling requirements for this system, however these systems fail to meet the 30 year MTBF, or 265,000 hours of continuous operation, requirement. The pumps that would be used in active cooling are driven by electric motors with insulation that has a typical lifetime between 20,000-25,000 hours under ideal environmental conditions [6]. The pumps are not only hindered by the insulation but also by the bearings. The typical lifetime of a L10 bearing in a low speed motor (60 RPM) is only 25,000 hours of operation. Even if extreme reliability bearings were within cost limits, they are only designed for use up to 200,000 hours. Without the bearings or insulation meeting the 30 year MTBF requirement, active cooling systems are eliminated as a possibility.

A passive thermal management system must be developed to provide the necessary cooling for the GCD-PAR due to the infeasibility of an active system. Heat must be dissipated through a single mounting plate since the power converter cannot be immersed. There is a 64 °C allowable gradient throughout the cold plate, from the 40 °C ambient to the 104 °C maximum allowable cold plate temperature. The simplest form of passive cooling is increasing the surface area for rejection to ambient air with the use of an extended fin array. The maximum baseplate flux that can be accomplished by a naturally cooled fin array with a 60 °C maximum baseplate differential is about 1 W/cm^2, based on the study of the limitations of pin fins in free convection by Fisher and Torrence [7]. Natural convection with the use of an extruded fin array will not supply sufficient cooling for the GCD-PAR system since the IGBT modules will require a baseplate flux of around 2.5 W/cm^2.

Many other methods of passively dissipating heat exist including magnetic cooling, thermoelectric pumps, single phase thermosiphon loops and heat pipes. The more advanced of the options are magnetic cooling and thermoelectric heat pumps. Magnetic cooling via the magnetocaloric effect has been widely studied since the 1970s, but there have been a large number of barriers preventing its commercial adoption. Some metals get warmer when exposed to a magnetic field and cool down when the magnetic field is removed. The magnetocaloric effect works by repeatedly introducing and then taking away a magnetic field from one of these metals to create a heat pump that moves heat from one location and brings it to another location. This method of cooling, however, is complex and requires expensive materials. Thermoelectric heat pumps operate on the Peltier effect. The Peltier effect, similar to the magnetocaloric effect, is a temperature gradient caused by applying a voltage between two electrodes connected to a semiconductor material. In this method, thermoelectric devices can be used to move heat from the IGBTs to an elevated temperature fin array. While this method is feasible, it is also complex and expensive. The coefficients of performance for commercially available heat pumps are below 1, which means it would take more power to drive the thermoelectric devices than there would be losses from the power converter.

Heat pipes are widely used for passive thermal management. They are utilized in the space industry, computer systems, solar thermal applications, permafrost cooling, HVAC systems and nuclear power conversion. These systems operate on a thermal cycle that transfers heat between two thermal reservoirs by the evaporation and condensation of a heat transfer fluid. As heat is input to the evaporator, the heat transfer fluid boils and becomes a vapor. This creates a pressure gradient along the heat pipe which forces the

vapor to flow along the pipe to the condenser. The vapor condenses back to a liquid, the liquid returns to the evaporator either through capillary action, centrifugal force or gravity, depending on the application, and the entire process repeats. Heat pipes are capable of dissipating heat fluxes higher than 10 W/cm^2 [8]. Two phase systems, while effective, create concerns for longevity due to their pressurized operation and capillary material degradation. This makes a heat pipe unnecessary for the desired application requiring a heat flux of 2.5 W/cm^2 and undesirable due to reliability concerns,

Single phase thermosiphons have been identified as a favorable solution for passively cooling power electronics. In 1973, Japiske showed the advantage of utilizing a closed-loop thermosiphon for cooling systems where noise or reliability was of concern. He showed successful use of a closed-loop thermosiphon to dissipate heat fluxes of about 2 W/cm^2. Loeffler et. al developed a model that optimized the design of a single phase closed-loop thermosiphon [9]. The thermosiphon was able to maintain a cold plate temperature of 100 °C by passively removing 5 kW, at a heat flux of 2 W/cm^2, from a 12" by 28" cold plate to ambient with the use of an oil filled radiator. Therefore, a single phase closed loop thermosiphon was selected as the best choice for the GCD-PAR thermal management system because it has been shown that this system is suitable for reliably dissipating similar heat fluxes.

1.4 Closed loop thermosiphons

A closed loop thermosiphon is an energy transfer method capable of transferring heat from a heat source to a heat sink utilizing buoyancy force and gravity. Closed loop thermosiphons have been used in variety of applications including the nuclear industry, the chemical processing industry, the energy conservation industry, the electronics

industry and internal transformer cooling [10-15]. As Welander documented in 1967, the fluid is driven by the pressure difference and buoyancy force and retarded by frictional forces [16]. As heat is added to the heat transfer fluid, the fluid expands and the density of the fluid decreases causing the fluid to rise. On the opposite side of the loop, the heat transfer fluid is cooled causing the density to increase. This causes the fluid to sink creating a continuous circulation of fluid as shown in Figure 4.

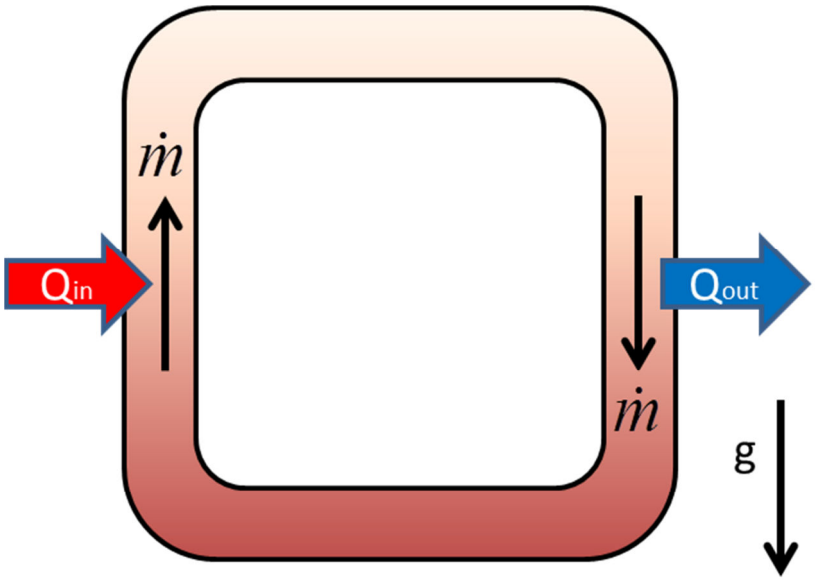

Figure 4. Schematic of single phase closed loop thermosiphon operation

In practice, a majority of electrical transformers are oil-immersed and cooled by natural convection to ambient. The heat generated from the core is moved to the tank walls and in some cases to radiators through the transformer oil, and is then returned to the ambient through natural convection. Many of the pole mount transformers, depicted in Figure 5, have enough surface area to reject the required heat load without the use of radiators.

Figure 5. 50 kVA single phase pole mount transformer [17]

Some transformers incorporate oil-filled fins extending out from the transformer body to increase surface area for natural convection and radiation to ambient. When additional heat rejection is required, like the 1 MVA transformer depicted in Figure 6, radiator banks are incorporated into the transformer tank. The number radiator banks and number of fins per bank is determined by the expected heat loss from the transformer core and the surface area required to dissipate that heat loss.

Figure 6. 1 MVA transformer with radiator banks for additional cooling [3]

Incorporating an additional single phase closed loop thermosiphon into these transformers would allow the power routers to be passively cooled by the oil already present in the transformer. This system will be utilized first in 50 kVA pole-top transformers and then incorporated into three-phase 13 kV transformers with up to 1 MVA of power flow control once the concept has been proven through the successful operation of the 50 kVA transformer. These assemblies will create two fluid loops: one going up through the additional thermosiphon to cool the power converter and one going up through the core of the transformer to cool the transformer coils. Both streams then combine while cooling down through the outer portion of the transformer tank in the case of the 50 kVA transformers and through the radiators in the case of the 1 MVA transformers. A schematic of the proposed 50 kVA dual loop thermosiphon assembly is shown in Figure 7. The red arrows in the schematic represent heat flow. Heat enters the system in the core of the transformer and from the converter which will be mounted to a baseplate. A fin array will be fixed to the baseplate to increase the surface area for cooling and allow more heat to be dissipated from the converter.

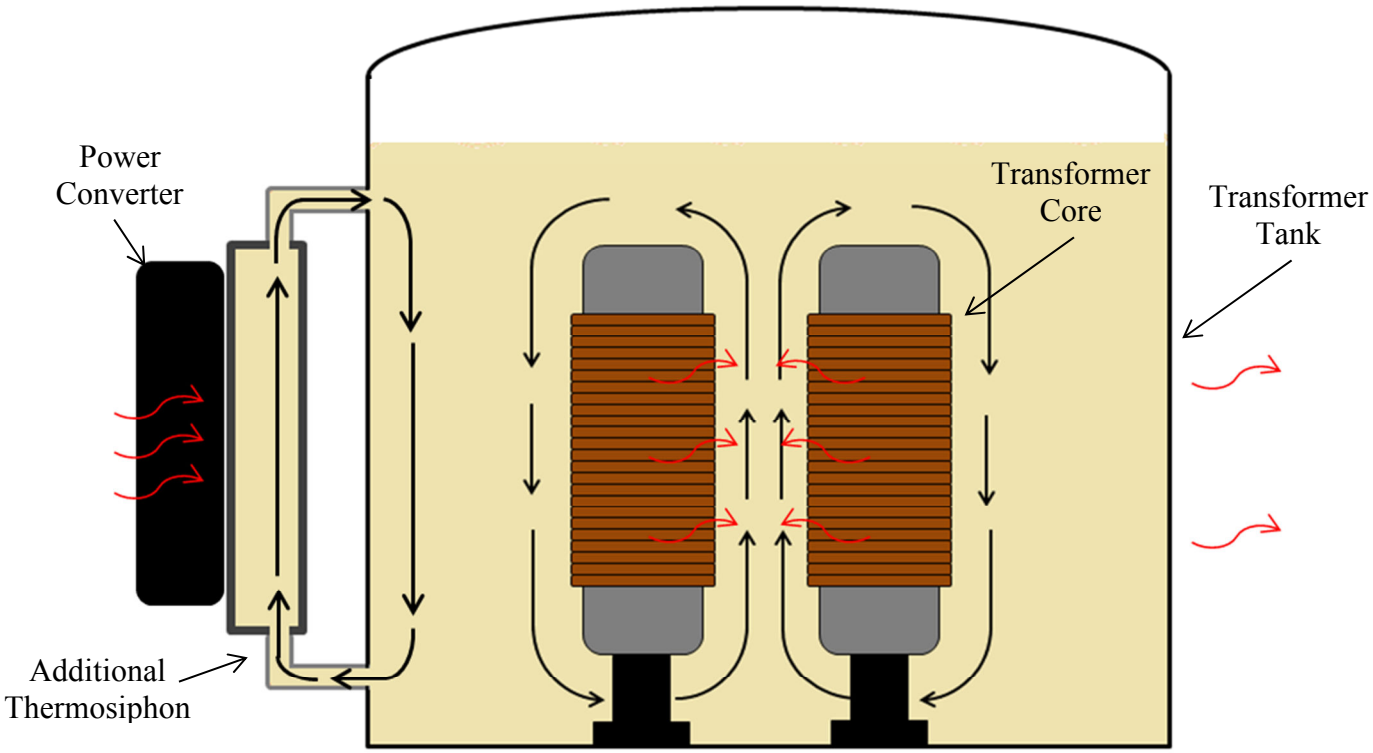

Figure 7. Schematic of the cross section of the 50 kVA pole mount thermosiphon-transformer assembly

The power router utilized for the 50 kVA assembly is slightly different from the electronics described in 1.2 for the GCD-PAR. For the 50 kVA assembly, the power router will be used to control less power than in the 1 MVA assembly and therefore will utilize different IGBTs, which have lower heat losses, and there will be no inductor losses. The IGBTs in this system lose a maximum of 40 W per device for a total loss of 80 W from the power router. The IGBTs also have a smaller device footprint giving them a similar heat flux. With an effective heat transfer area of 13.2 cm^2 for each IGBT, the heat flux that needs to be dissipated is 3.03 W/cm^2. With a similar heat flux and the same maximum operating baseplate temperature, the same method of cooling, a dual-loop single phase thermosiphon, will be utilized for both designs.

A model needs to be developed to describe the steady state operation of a dual-loop single phase thermosiphon to ensure that the proposed design will be able to keep the baseplate below the maximum operating temperature of 104 °C. There has been a great deal of effort put into modeling and describing the steady state operation of single loop single phase thermosiphons, but two thermosiphon loops have never been coupled so there has been no previous modeling or experimentation on this type of assembly.

The model needs to take in heat inputs and geometric parameters such as fin array dimensions and pipe dimensions to solve for critical temperatures throughout the thermosiphon-transformer assembly. Finite element CFD analysis has the potential to solve the steady state behavior of the given 50 kVA assembly, but would require too much time and computing power to solve. With a CFD analysis any change in geometry would require the model to be rebuilt, re-meshed and then solved again. This is computationally expensive and undesired for an initial prototype design. Numerical methods that require detailed geometric meshes create similar issues with time to solve and inability to have flexible geometric parameters. Therefore, an analytical model of the dual-loop single phase thermosiphon needs to be developed that can rapidly solve for the steady state operation given the heat inputs and geometric parameters. A detailed literature review, presented in Chapter 2, shows that two single phase thermosiphon loops have never been coupled to utilize the same cooling path and heat transfer fluid. Therefore, there has been no modeling effort into such a system.

This work will develop a thermo-fluidic analytical model that describes the steady state operation of a 50 kVA transformer augmented with an additional thermosiphon used to cool grid level power electronics. The analytical multi-physics thermosiphon model

couples existing fluid dynamic and heat transfer correlations to create a description of the steady state operation of a specific dual-loop thermosiphon design. Geometric parameters can be varied in the model to rapidly solve for the steady state operation of different designs to see if they are feasible. The validity of the model will be tested experimentally and the knowledge from those results will be utilized to design a thermosiphon-transformer assembly for a three-phase 13 kV transformer with up to 1 MVA of power flow control. These transformer-thermosiphon assemblies will make the GCD-PAR grid implementable to increase the potential for a successful, efficient smart grid.

This work shows how thermosiphons can be incorporated into grid assets that utilize a thermal reservoir to also cool power converters. An analytical model is developed to describe the steady state operation of 1 MVA and 50 kVA transformers augmented with thermosiphon assemblies. This model can be augmented to any grid asset containing a thermal reservoir with a thermosiphon assembly by modifying the heat inputs and pressure loss coefficients. The model can also be modified to account for varying ambient temperatures and radiative loads. The analytical model can quickly and accurately solve for the steady state temperatures of grid distribution assets augmented with thermosiphon assemblies.

Chapter 2 provides a detailed literature review of thermosiphon research and application. Chapter 3 details the development of the analytical thermo-fluidic model and the experimental validation of the model. Chapter 4 presents the detailed design method and final design for the augmented three-phase 13 kV transformer. Chapter 5 provides a summary of the work, conclusions, contributions and recommendations for future work.

CHAPTER 2

LITERATURE REVIEW

This chapter presents literature for both experimental and theoretical research completed for single phase thermosiphon operation. Single phase thermosiphons offer a quiet and reliable solution for transferring heat from both the transformer core and power electronics to ambient. Single phase thermosiphon application and operation have been heavily researched. There are four primary configurations found in the literature for single phase thermosiphons: open cavity, closed cavity with toroidal flow, closed cavity with horizontal heated sections and closed cavity with vertical heated sections. Thermosiphons have been utilized in a wide variety of applications including solar water heaters, thermosiphon reboilers, geothermal systems, nuclear power plants, emergency cooling systems in nuclear reacting cores, electrical machine rotor cooling, gas turbine blade cooling, thermal diodes, and electronic device cooling. The application that will be focused on in this work due to its relatability and applicability to this work is transformer cooling.

2.1 Open cavity thermosiphons

Open cavity thermosiphons, as depicted schematically in Figure 8, are useful for extremely small or extremely large systems. This system would be particularly advantageous in the case of an emergency in a nuclear reactor when it is imperative to discharge large amounts of energy quickly. The reactor could be cooled with an open cavity thermosiphon connected to a common industrial water supply located on the building roof. This would form a natural reservoir for an open cavity thermosiphon and would allow the expulsion of a large amount of energy. Another incentive to studying open cavity thermosiphon is that many of the phenomena observed in the open cavity

system are helpful in understanding other free convection internal flow processes and the knowledge can also be applicable to closed cavity thermosiphons.

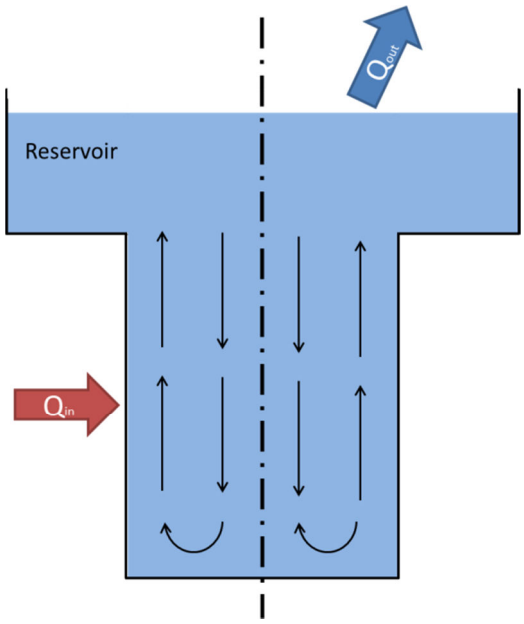

Figure 8. Open cavity thermosiphon

In 1971, Japiske and Winter published an analytical study of laminar boundary layer heat-transfer in open thermosiphons [18]. The study produced a Nusselt correlation along with analytical results that were within 1% of the experimental data. The proposed GCD-PAR cooling will utilize existing transformer oil and will be incorporated into the grid so an open cavity solution is not feasible for this application. The large volume of heat transfer fluid necessary for the power reservoir, and the associated footprint limitations, substantially increase the cost point of the open cavity system over the closed cavity solution, leading the broad adoption of the closed systems.

2.2 Closed cavity toroidal thermosiphons

Closed cavity toroidal thermosiphons are described by a torus, shown in Figure 9, oriented in the vertical plane and containing a heat transfer fluid. The fluid is driven by

the distribution of temperature around the walls or by an internal heat source. The studies of toroidal thermosiphons consider either a known heat flux over part of the loop and convective cooling with a constant heat transfer coefficient and known wall temperature over the rest, known heat flux over the whole loop or convective heat transfer with constant heat transfer coefficient and known wall temperature over the whole loop [19].

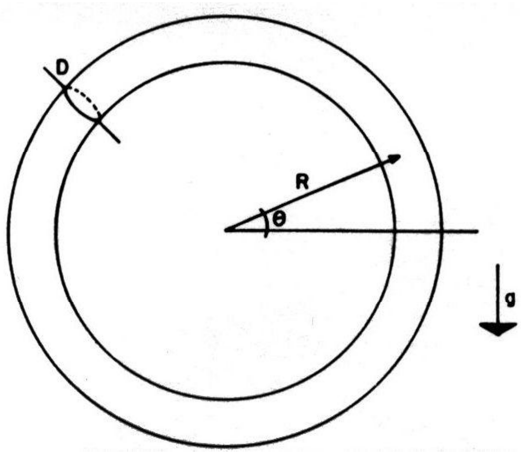

Figure 9. Closed loop toroidal thermosiphon

In 1975, Creveling et al. studied a toroidal configuration with a constant wall flux inward [20]. They found that steady flow solutions of the 1-D model equations agreed with experimental findings if the wall-stress parameterization in terms of the mass flux varied with the applied heating rate. Four years later, Greif et al. integrated the 1-D thermosiphon model, used by Creveling, with linear drag using a finite-difference representation to obtain further information about the predicted transient behavior of the simple loop [21]. Damerell and Schoenhals studied the predicted and observed steady flow, as well as the observed flow instability in a system where the symmetry axis of heating and cooling was slanted with respect to gravity [22]. In 1983, Hart conducted a theoretical study of the nature of motions in a toroidal fluid loop oriented in the vertical plane and subject to internal heating and/or thermal wall conditions [23]. Mihir, Ramos

and Trevino discussed the behavior of a toroidal thermosiphon with known heat flux around the loop in 1984 [19]. They reduced the problem to a set of three ordinary differential equations to solve the behavior of the flow. The converters used in this study are planar circuit boards necessitating a planar cold plate which makes the toroidal configuration infeasible.

2.3 Closed cavity thermosiphons with horizontal heated sections

There has been considerable work into describing the flow and the stability of closed cavity thermosiphons with horizontal heated sections, as depicted schematically in Figure 10. Most theoretical thermosiphon work is based on the assumptions made by Welander in 1966 [16]. This was the first publication considering the fluid to be driven by the pressure difference and buoyancy force and retarded by frictional forces. This work examined the irregularity of flow in the closed loop thermosiphon with horizontal heated sections. Welander's assumptions included the Boussinesq approximation, the tangential friction force on the fluid is proportional to the instantaneous flow rate, the temperature of the fluid is uniform over each cross sectional area and the heat transfer between the pipe and the fluid is proportional to the difference between prescribed wall temperature and the fluid. The Boussinesq approximation refers to the temperature dependency of the density of the heat transfer fluid with respect to gravity, while assuming the fluid is otherwise incompressible with regard to inertial effects in flow. These assumptions allowed for 1-D approximations for a single phase fluid.

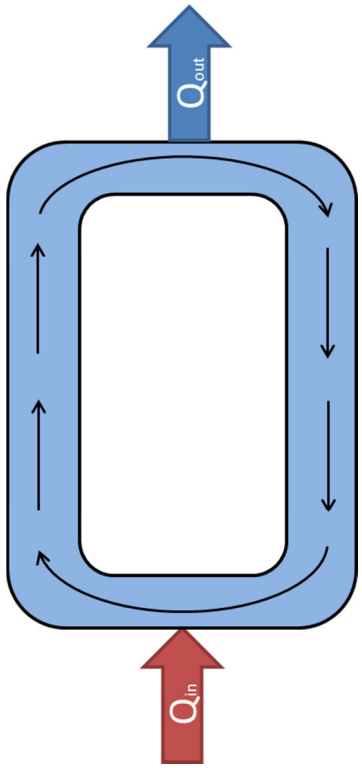

Figure 10. Closed loop thermosiphon with horizontal heated sections

In addition to his work in open thermosiphons, Japiske also published an evaluation of a closed cavity thermosiphon for potential application in turbine blade cooling in 1970. The lower walls of the closed cavity thermosiphon were heated while the upper walls were cooled. Japiske made flow observations using dye traces and collected spatial temperature measurements to determine experimental Nusselt numbers for describing the heat transfer achieved by the thermosiphon. Experiments were run with various cavity inclinations with the conclusion that inclination induced circulatory flows which improved the heat transfer performance of the thermosiphon.

In 1981, Zvirin presented theoretical and experimental results in natural circulation loops with horizontal heated sections. This study also detailed modeling methods to describe steady state flows, transient flows and stability characteristics [24]. In 1985,

Mertol and Greif gave a review of transient, steady-state and stability behavior of different thermosiphon configurations under various conditions and compared them to experimental results [25].

In 2002, Ishihara et al. conducted an investigation comparing flow visualizations to finite element predictions in a closed loop thermosiphon. Unlike the schematic in Figure 10 with heat transfer on opposing lengths, Ishihara et al. studied a thermosiphon with symmetric heating and cooling sections with the lower portion heated and the top portion cooled. The study concluded that varying the combination of cavity geometries and temperature differences resulted in different convection regimes and stability [26]. In 2004, Ishihara and Nakagawa conducted experiments to further study the flow characteristics in a closed cavity thermosiphon with horizontal heated sections. They used three kinds of silicon oil to study the interaction between the upward and downward flows showing that higher Rayleigh numbers result in multi-branched flow [27].

In 2003, Maiani et al. developed a parametric, analytical model for the stability of a fluid loop with the lower section heated and upper section cooled. This work incorporated the Boussinesq approximation into fluid and energy balances to describe the operation of the fluid loop [28]. In 2005, Burroughs et al. determined the theoretical stability behavior of a thermosiphon heated from below by performing a mathematical analysis of Navier-stokes equations in the Buossinesq approximation. The mathematical analysis was compared to a 3D FEM CFD code of much higher complexity and reports close agreement. Burroughs et al. established assumptions used to simplify the evaluation of thermosiphon operation [29].

In 2002, Vijayan published an investigation of the fluid flow through a rectangular fluid loop with the bottom section heated. Vijayan related the Reynolds number to the Grashoff number and two constants and through experimentation was able to fully develop correlations for fully developed laminar and turbulent flow [30]. In 2005, Vijayan et al. compared the dynamic behavior of the single-phase and two-phase thermosiphon loop with conventional tube and different placements of the heater and cooler. The study concluded that the most stable configuration of the thermosiphon loop with conventional tube is the one with both vertical cooler and heater [31].

In addition to the findings by Vijayan that vertical heated sections create the most stable thermosiphon loops, the power routers are required to be in a vertical orientation making the horizontal heated thermosiphon orientation infeasible. Unlike the horizontal heated thermosiphons, stability behaviors are not a concern in the vertical heating orientation. Although the horizontal orientation literature is not directly relatable to the proposed setup for the GCD-PAR, the methods for describing the flow, model assumptions and experimental techniques are relevant to this work.

2.4 Closed loop thermosiphons with vertical heated and cooled sections

Closed loop thermosiphons with vertical heated sections, as depicted schematically in Figure 11, are directly relatable to the proposed set up for the GCD-PAR. This orientation has been studied extensively particularly in the use of solar water heaters and transformer cooling. In 1954, Hamilton and Palmer studied fluid flow and temperature profiles in thermosiphons which they called “thermal convection harps”. The researchers utilized a method of predicting the Reynolds modulus based on wall temperature measurements, assuming fully developed, laminar flow. This work built off of the

method employed by Welander by integrating the buoyancy potentials and friction terms to solve for the fluid flow rate and Reynolds number. A velocity profile was calculated by iteratively solving for the Reynolds number and heat transfer equations. The model performance was validated with an experimental thermosiphon built from Pyrex tubing. One vertical section was heated by a water jacket while the opposite vertical section was cooled by a water jacket. The model was found to predict the Reynolds number to within 30% accuracy [32].

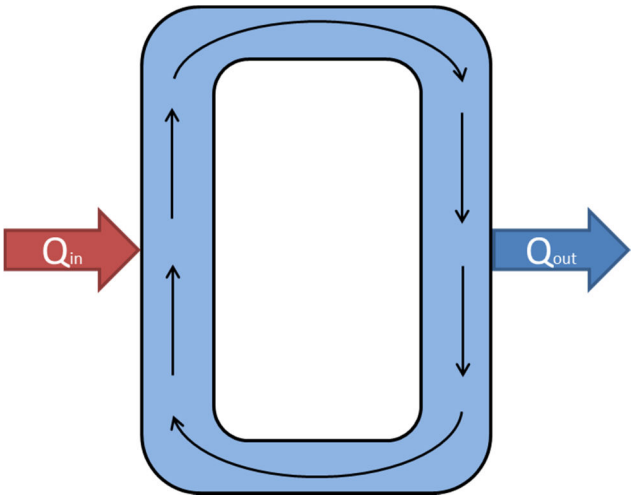

Figure 11. Closed loop thermosiphon with vertical heated and cooled sections

In 1962, Close published work seeking to predict the performance of the thermosiphon operation in solar water heaters [33]. Utilizing an insulated tank and manifold allowed the flow rate throughout the system was able to be estimated by using just the internal energy of the water and pressure losses throughout. The pressure losses throughout the system were estimated using established pipe flow correlations and all temperature gradients were assumed to be linear. Close's model was able to predict the mid-day temperatures of specific points in two real life solar water heaters to within 10

°C. This method of solving the temperatures throughout a thermosiphon is applicable to this work.

In 1974, Ong presented the theoretical performance of a solar water heater utilizing thermosiphon flow which was evaluated with a finite-difference solution procedure [34]. Ong improved Close's model by including temperature dependency into the fluid dynamic and heat transfer correlations. He conducted experiments on an experimental heater which utilized a flat-plate collector design. In these experiments, he measured water mass flow rates at half-hour intervals using a dye-injection method. The dye was injected into the flow stream at the beginning of a clear length of tube and the time it took to travel from that entrance to a known distance was measured. The temperature distribution was measured continuously throughout the experiment. In 1976, Ong presented an improved model by splitting the solar heater into sections [35]. This allowed the separate sections of the thermosiphon: the collector, the manifolds and the tank to be evaluated separately. An energy balance, heat transfer analysis and fluid flow analysis was performed on each individual section. This also allowed each section to be evaluated at its mean temperature instead of an overall mean temperature. The changes implemented in this work improved the predictions for both the fluid temperatures and velocities. While the finite difference method used in this work gave accurate transient thermosiphon operational predictions, it also took a long time to solve. The assumptions and separation methods used by Ong can be utilized in the modeling of the dual-loop thermosiphon-transformer assembly.

In 1992, Bernier and Baliga published an investigation of the flow velocities in a closed loop thermosiphon with the vertical sections heated and cooled and a uniform

cross section throughout. To avoid errors resulting from assuming average temperature and velocity profiles, the researchers developed a 1-D/2-D model. The insulated sections of the loop were described using 1-D correlations which were then coupled with 2-D cylindrical coordinate models used to solve for the heat transfer sections. The model was validated with the use an experimental thermosiphon containing extended heating and cooling sections on vertical legs connected via uniform cross section, insulated pipe with 180° bends at the corners The experiments showed the model predicted flow rates were within 5% of the experimental values [36].

In 1993, Polentini et al. conducted experiments cooling an array of discrete heat sources in a closed rectangular cavity filled with water and then filled with an engineered dielectric as the heat transfer fluid. The heat sources, arranged in a 3 x 3 array, were placed on one of the vertical walls while the opposite vertical wall contained a heat sink maintained at lower temperature. Throughout the experiments, the aspect ratio and inclination of the cavity were varied. The researchers discovered that the aspect ratio of the cavity did not change the heat transfer performance of the thermosiphon, but moving the heat sources from vertical to a lower horizontal orientation resulted in unsteady flow and increased heat transfer [37].

In 2011, Bielinski and Mikielewicz presented a detailed analysis of heat transfer and fluid flow in single phase and two phase closed-cavity thermosiphons with varying locations for heat loads and cooling with constant cross-sectional area throughout the loop. The model developed allows the selection of one, two or three heat sources at any location in the bottom horizontal pipe or in the vertical legs. The heat sink allows the same variability except the locations must be anywhere on the top horizontal pipe or on

the vertical legs. The researchers consider constant cross section area per heated and cooled length. The following assumptions were made by Bielinski and Mikielewicz for single phase flow:

- Thermal equilibrium exists at any point of the loop
- Incompressibility because the flow velocity is relatively low compared to the acoustic speed of the fluid
- Viscous dissipation in the fluid is neglected in the energy equations
- Heat losses in the thermosiphon loop are negligible
- $(D/L)<<1$ therefore 1-D models are used and the flow is fully mixed. The velocity and temperature variation at any cross section is therefore neglected
- Heat exchangers in the thermosiphon loop can be equipped by conventional tubes or minichannels
- Fluid properties are constants, except density in the gravity term

The researchers analyzed trends and relayed which orientations were suitable for different applications but the model had not been experimentally validated so the accuracy of the models is unknown [38].

In 2012, Rosen, Dam and Mattheij studied the optimal wall-shape design of single phase laminar thermosiphon loops. Solving the governing equations using a finite element method, they characterized the effects and amplitude of the ratio of expansion and contraction in the thermosiphon loop and also showed that given a fixed amplitude there was an optimal ratio of expansion and contraction that minimizes the temperature inside the thermosiphon and optimizes its performance [39].

Dobson and Ruppersburg published an investigation into single phase and two phase closed loop thermosiphons with vertical heat transfer sections for use in cooling of the reactor cavity of a Pebble Bed Modular Reactor in 2007. The flow was determined by performing a momentum balance around the entire loop and a thermal circuit approach was used to solve the heat transfer into and out of the loop [13]. Part II of the paper performed experimented to find the heat transfer coefficients used in the thermal circuits [40]. These papers detail the development of an analytical thermosiphon model and the design of an experimental thermosiphon.

Loeffler [23] expanded upon the work done by Dobson and Ruppersburg by allowing for changes in internal geometries throughout the thermosiphon and creating an optimization from the analytical model. Loeffler developed a model that optimized the design of a single phase closed loop thermosiphon [41]. The thermosiphon was able to maintain a cold plate temperature of 100 °C by passively removing 2.5 kW from a 12" by 28" cold plate to ambient with the use of an oil filled radiator. Device mounting temperatures were found to be within 1.1 °C of model predictions and system thermal resistances were within 2% of their predicted values. The maximum fluid temperature disagreement was found to be 8 °C.

2.5 Transformer cooling

Outside of solar water heaters, transformer cooling is one of the oldest commercial applications utilizing the principle of buoyancy driven flow. Transformer core losses must be rejected to ambient to prevent overheating of the windings and premature insulation failure. Transformers utilize passive thermal management methods due the grid implementation requirements for reliability. General transformer cooling and design is

standard practice in industry. Standards have been developed by IEEE for transformer loading and life ratings [42]. In 1944, Pierce updated the IEEE Loading Guide for Miner-Oil-Immersed Transformers with a program that performed transformer loading calculations. The update also included changes to the equations for fluid flow, thermodynamics and heat transfer as well as accommodations for transient loading. This was particularly important for predicting hot spots during overloads. The significance of this work to the current study is its implementation of analytical modeling of thermosiphon cooling and development of a code that predicts liquid filled transformer loading capacity based in limiting winding, insulation and oil temperatures [43]. Extensive research has been published on modeling the heat transfer within transformers and predicting limiting hot spot temperatures. This is not an extensive literature review on transformer cooling, but specific papers will be highlighted due to their relevance to the present work.

In 1958, Kunes measured temperature and velocity profiles in an experimental thermosiphon for transformer cooling. Kunes studied the effect of the vertical position of the heated coils on the temperature and velocity profiles. Research concluded that the lower vertical positions of the heated coils in the tank induced qualitatively greater oil circulation.

In 1980, Oliver presented a network method for predicting the flow paths and temperature distribution of oil throughout transformers [44]. Oliver created a nodal network constructed throughout the cooling ducts within and around the windings. The Nusselt numbers and friction factors were predicted by assuming laminar flow throughout and using existing correlations. While this paper only applies this nodal

network method to transformer design, it can be applied to any network of flow paths like that which will be seen in the GCD-PAR.

In 2001, Vecchio developed a thermal model to capture the physical processes occurring within a transformer [45]. This model utilized a nodal network of oil pressures, velocities and temperatures to predict performance by iteratively solving a non-linear system of governing equations. *Transformer Design Principles*, the book Vecchio published with his findings, is significant to this research by showing the possibility of developing and solving a system of non-linear equations completely describing the thermo-fluidic system.

Published in 2004, Swift et al. created an analytical model that simplified the calculation of transformer hot spots and thermal performance with the use of thermal circuit equivalents. In the thermal circuits, the temperature difference acted as the voltage, the thermal load acted as the current, the thermal resistance acted as the impedance and the thermal capacitance of the fluid acted as a storage element [46]. In a follow up paper also published in 2004, Swift et al. tested the validity of their model by performing 24 hour experiments in both the summer and winter measuring the top fluid temperatures in transformers. These top fluid temperatures varied less than 5 °C from the model predictions [47]. This work is significant because of its use of 1-D thermal circuits to successfully model thermosiphon operation.

From 2012 to 2015, there have only been eight papers published with the search criteria thermosiphon and power electronics. From these eight papers, six of the papers focus on two phase flow which is not of interest to this work due to the reliability concerns [48-53]. Another of the papers presents a thermoelectric mini cooler coupled

with a micro thermosiphon for CPU cooling which does not have any particular significance to this work [54]. In 2012, Kang presented a review of advanced cooling in power electronics [55]. He mentions thermosiphons utilizing liquid cooled plates as an option but does not add any new insight into the space.

2.6 Research Objectives

While extensive research has been completed on both closed loop thermosiphons with vertical heat sources and modeling thermosiphon flow in transformers, no literature was found directly pertaining to the pursuant work. The research objectives for the present work are:

- To develop a thermo-fluidic analytical model for transformers augmented with secondary flow path thermosiphons;
- To validate the analytical thermo-fluidic model approach for different geometric configurations and thermal loads;
- To design a thermal management system to passively cool power electronics by augmenting transformers with single phase thermosiphons to use the existing transformer oil to also cool the power electronics.

CHAPTER 3

50 KVA DUAL-LOOP THERMOSIPHON-TRANSFORMER ASSEMBLY

3.1 Introduction

This chapter presents a single-phase thermosiphon coupled to a 50 kVA transformer for power electronics cooling. This design includes a secondary-loop cooling path that utilizes the cooling oil already present in the transformer to also cool the power router. An analytical thermo-fluidic model is developed that couples existing fluid dynamic and heat transfer correlations and thermodynamic principles to create a description of the steady state operation of a specific dual-loop thermosiphon design. The model must take in heat inputs and geometric parameters from the thermosiphon and transformer to accurately predict the junction temperatures for the power electronics mounted to the cold plate. This thermosiphon design is then manufactured and tested. The experimental data is then compared to the results from the analytical model to verify its accuracy.

3.2 General Problem Statement

This chapter considers a thermosiphon that is incorporated into a 50 kVA pole top transformer as illustrated in Figure 12. Buoyant forces drive oil up through the thermosiphon and transformer core and down around the outside of the transformer tank.

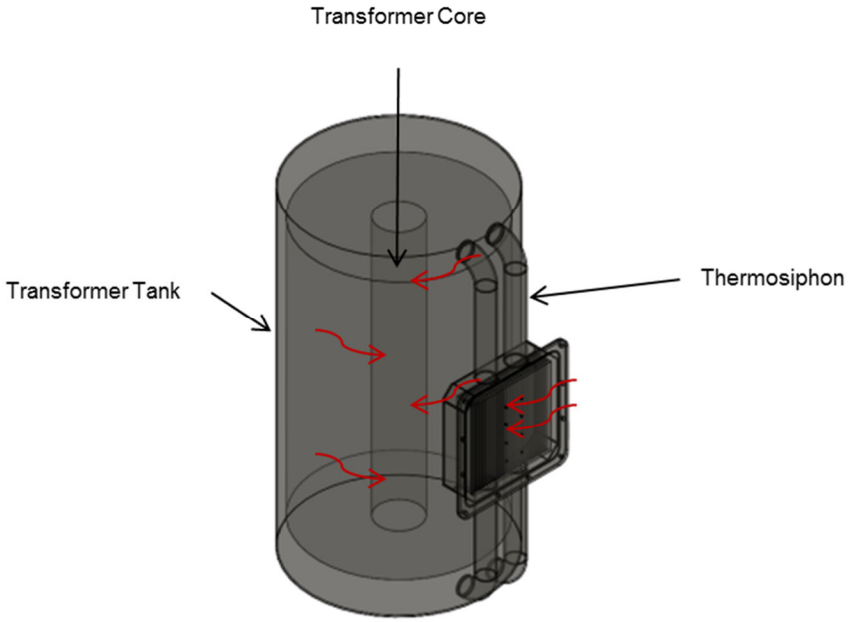

Figure 12. A solid model of a typical 50 kVA transformer as will be considered in this study

The red arrows represent heat flow. Heat enters the system in the core of the transformer and from the converter which will be mounted to a baseplate. A fin array fixed to the baseplate increases the surface area for cooling and allows more heat to be dissipated from the converter. The transformer consists of the tank, the core, and the coils. The thermosiphon, illustrated in Figure 13 , consists of the upper and lower manifolds, the plenum, the fin array, baseplate, and the power converter which is not depicted but will be mounted to the baseplate.

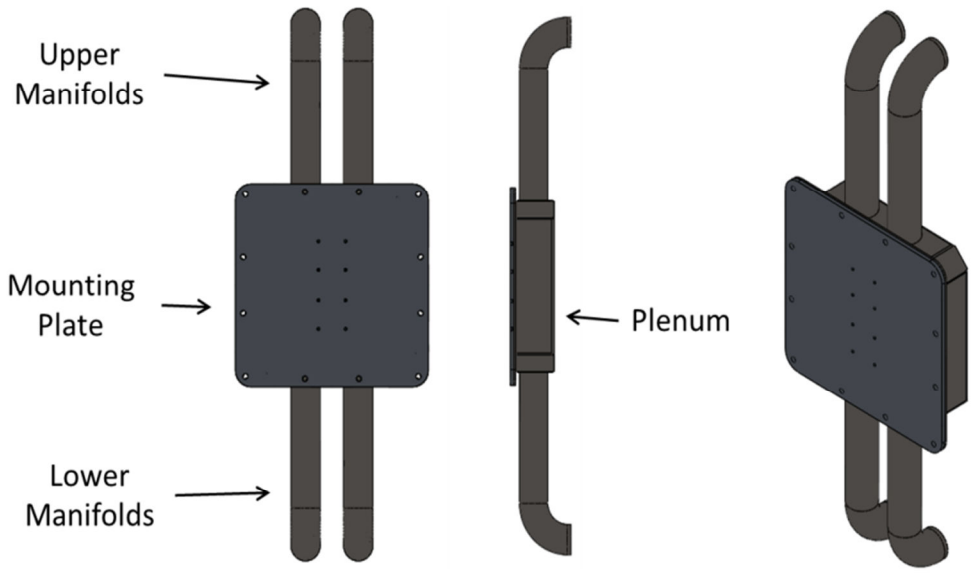

Figure 13. CAD model of the 50 kVA thermosiphon

The geometry will be simplified to consider three heat transfer planes: transformer heat input, converter heat input and combined ambient rejection. A 1-D thermal analysis, results compiled in Table 1, was completed to determine the maximum operating temperature for the cold plate. A conservative approach was taken by assuming the maximum power dissipation for the module occurred in both the IGBT and the diode. The thermal resistance for the IGBT and diode were taken from the IGBT module's data sheet. The maximum allowable baseplate temperature determined by the diode is 104°C.

Table 1. Maximum baseplate temperature at maximum loss

Metrics	Units	IGBT	Diode
Limiting $T_{junction}$	[°C]	150	125
Max loss/junction	[W]	300	300
Thermal Resistance	[°C/W]	0.038	0.068
$T_{baseplate}$	[°C]	113.6	104.6

Additional key specifications for the system, compiled in Table 2, include the maximum transformer loss, ambient temperature and geographic location for operation.

Table 2. Key design specifications for 50 kVA unit

Metrics	Value
Maximum total loss from transformer	700 W
Maximum T_{amb}	40 °C
Location for operation	Southeast

The model is developed so that geometric parameters and heating loads can be varied, solving for the steady state operation in less than 0.1 seconds.

3.3 Model Assumptions

The dual-loop single phase thermosiphon-transformer assembly is divided into seven sections as depicted schematically in Figure 14. These sections are treated as independent segments such that thermodynamic, fluid dynamic and heat transfer analysis can be applied to the segments individually. A first law thermodynamic energy balance is maintained through each of the seven sections. Temperature dependent properties are defined by the mean temperature between the temperature of the fluid entering a section and the temperature of the fluid exiting the section. It is assumed thermal equilibrium exists at any point of the loops and mass accumulation is zero. The ratio of the hydraulic diameter to the length is also much less than one so the flow is assumed to be fully mixed and temperature variation at any cross section is therefore negligible.

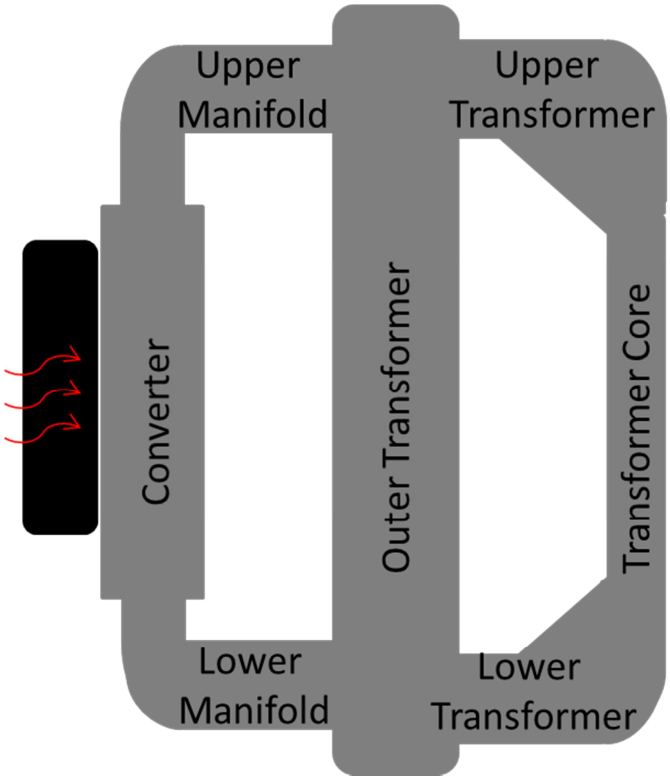

Figure 14. Schematic of thermosiphon-transformer assembly

Incompressibility is assumed due to the relatively low flow velocity compared to the acoustic speed of the fluid which allows the use of the Boussinesq approximation. Due to the low flow rates, incompressibility of the fluid, and small heat transfer layer gradients, second law irreversibilities are assumed to be negligible. The Bernoulli streamline pressure equation is utilized for the fluid dynamic description. Viscous dissipation in the fluid is neglected in the energy equation thereby avoiding the added computation complexity of numerical solutions to the governing differential equations.

3.4 Modeling Approach

The flow throughout the thermosiphon-transformer assembly is analogous to the flow of current through a circuit. The buoyancy gains are treated as voltage sources, the pressure losses are treated as resistors and the mass flow rates are treated as the current.

Utilizing these analogies, the circuit for the dual loop thermosiphon is illustrated in Figure 15.

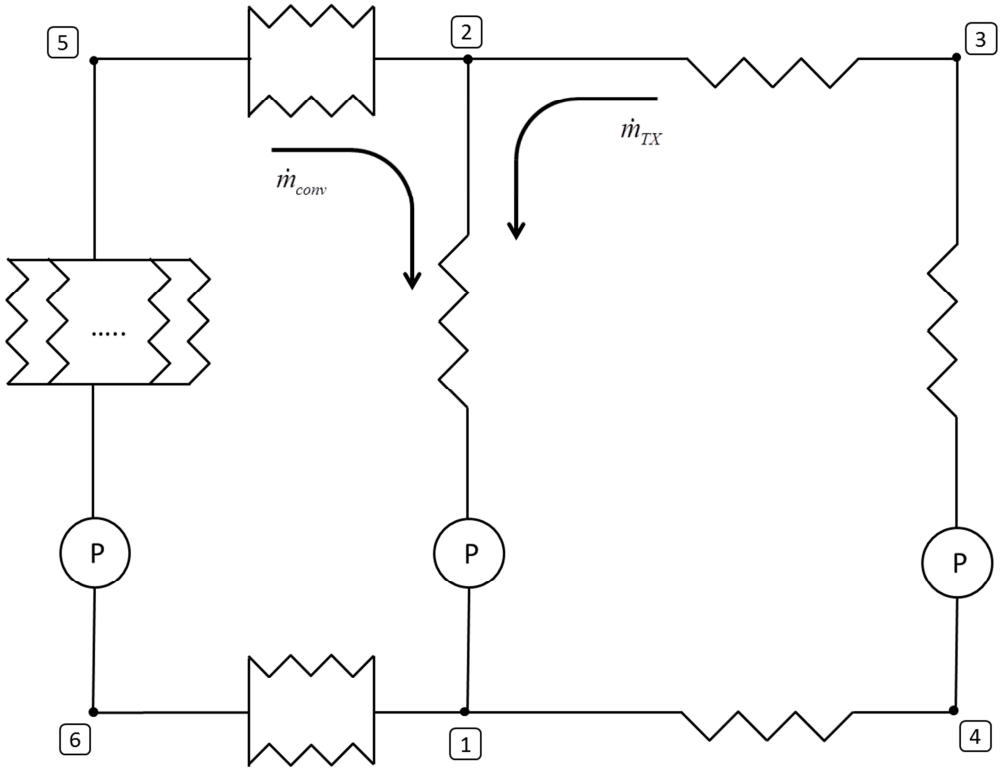

Figure 15. Fluid circuit for the 50 kVA thermosiphon assembly

The numbers at each node represent the location at which the temperature of the fluid will be analyzed. Location 1 is the bottom of the transformer tank. Location 6 and 4 are the bottom of the lower manifold and bottom of the transformer core, respectively. The temperature at these locations is considered the same as location 1. Location 2 is the top of the transformer tank, location 3 is the top of the transformer core and location 5 is the top of the upper manifold. The resistors in Figure 15 represent the pressure losses and the buoyancy gains are represented by the circles. The figure illustrates the flow of the fluid up through both the converter and transformer core and down through the transformer tank. Meshed network analysis along with thermodynamic principles is used to solve the

mass flow rates and the temperatures throughout the system. In this analysis conservation of mass is utilized to ensure that the two pressure loops are balanced. The key inputs to the model are the geometric parameters (diameter of the tank, diameter of the core, length and radius of the upper and lower manifolds, etc.), the heat input from the transformer, the heat input from the power routers and the ambient temperature outside the transformer. The geometric parameters are important in defining the flow losses through the system.

3.5 Analytical model development

Fluid flow through the dual-loop thermosiphon is driven by the balance of buoyancy pressure potentials across the vertical sections, due to thermal expansion, and pressure drops due to flow losses throughout. The power electronics devices are discrete heat sources arrayed on the cold plate. The model imposes an isothermal cold plate boundary condition and aggregates the discrete heat loads into a total dissipative load for the converter that is convected into the fluid. From node 5 to node 6, heat input from the converter decreases the density of the fluid causing it to flow upward. Similarly, the heat input from the transformer core causes the fluid to flow up from node 4 to node 3. The fluid is cooled on the outside of the transformer tank causing the density to decrease and flow is induced from node 2 to node 1. Equations (1) - (5) are taken from Okiishi's *Fundamentals of Fluid Mechanics* [56]. The buoyancy potential across the vertical sections is given by Equation (1).

$$\Delta P_{buoy} = \beta \rho g L \Delta T \qquad (1)$$

The pressure losses through the system are the sum of all major and minor losses incurred as show in Equation (2).

$$\Delta P_{loss} = \sum \Delta P_{major} + \sum \Delta P_{\min or} \qquad (2)$$

The major losses through the modified transformer are determined with established methods and given by Equation (3) for rectangular channels and Equation (4) for circular channels.

$$\Delta P_{major} = \frac{12\mu L}{bh^3}\left(\frac{\dot{m}}{\rho A}\right) \qquad (3)$$

$$\Delta P_{major} = \frac{12\mu L}{\pi \cdot r^4}\left(\frac{\dot{m}}{\rho A}\right) \qquad (4)$$

The flow through the assembly is assumed to be laminar, which is confirmed when the mass flow rates are solved. Minor losses occur when a fluid encounters a change in flow area or flow direction. The minor pressure losses are calculated using Equation (5).

$$\Delta P_{\min or} = \frac{K_{loss}\rho}{2}\left(\frac{\dot{m}}{\rho A}\right)^2 \qquad (5)$$

The loss coefficients, K_{loss}, are different for each flow situation. The flow into and out of the lower and upper manifolds in the thermosiphon is modeled as the flow entering and leaving a T-junction. The change in flow direction is depicted in Figure 16 with their respective loss coefficients [56].

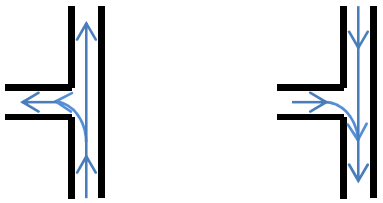

$K_L = 1.4$ $K_L = 1.7$

Figure 16. Loss coefficients for flow entering and leaving the thermosiphon

The flow losses for the 90° bends throughout the assembly are determined via plots of the loss coefficient as a function of the bend radius, pipe diameter and surface roughness [56]. The flow losses for the expansion into and out of the upper and lower manifold piping and into and out of the transformer core were determined with similar plots with the loss coefficient as a function of the change in area.

Kays performed a study in 1950 on the pressure loss in abrupt changes in cross section at low Reynolds numbers [57]. He graphically presented loss coefficients as a function of the area ratio across the flow transition for a range of Reynolds numbers. This model will incorporate polynomial curve fits to data taken from the laminar plots for the appropriate expansions and contractions. The area ratio σ is calculated using Equation (6).

$$\sigma = \frac{A_{small}}{A_{large}} \qquad (6)$$

The equations for the loss coefficients for contraction into the fin channels is given by Equation (7) and for expansion out of the fin channels is given by Equation (8).

$$K_{cont} = -0.3835\sigma^2 - 0.0245\sigma + 1.2 \qquad (7)$$

$$K_{exp} = 0.988\sigma^2 - 2.77\sigma + 1 \quad (8)$$

Idel'chik performed a study to determine the loss coefficients for various piping and duct geometries. One of the geometries studied was the transition from a rectangle to circle and vice versa [58]. The loss coefficient is plotted as a function of geometric parameters in the transition such as the length of transition. This plot was used to determine the loss coefficient for the fluid entering and leaving the core.

There exist different internal geometries for the 50 kVA transformer cores that will vary the major and minor pressure losses. The transformer used in this study has an internal cylindrical core that the heat transfer fluid flows through with a baffle raised from the opening of the cylinder. To account for this baffle, a correlation derived by Idel'chik for disk valves, as depicted in Figure 17, is used.

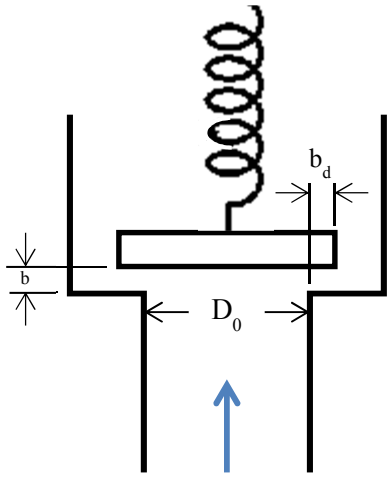

Figure 17. Schematic of disk valve used for baffle correlation

The minor losses along each flow path are summed to obtain the total pressure loss as the result of minor losses along the path. Integrating the pressure gradient along each flow path must result in a net pressure change of zero and is given by Equation (9).

$$\sum \Delta P_{buoy} - \sum \Delta P_{major} - \sum \Delta P_{minor} = 0 \quad (9)$$

The change in temperature between each node of the fluid circuit is determined with a first law energy balance. The heat flow is governed by Equation (10).

$$Q = \dot{m} c_p \Delta T \quad (10)$$

A thermal circuit, as depicted in Figure 18, is utilized to describe the heat transfer from the inside of the transformer tank to ambient.

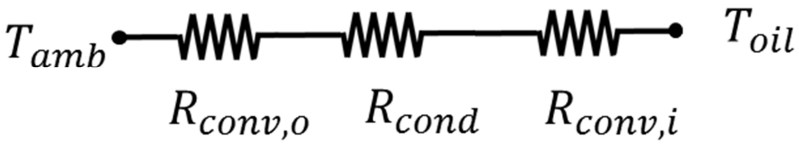

Figure 18. 1-D thermal circuit describing heat transfer from the oil to ambient

The convective resistances and conductive resistance are determined via Equations (11) and (12), respectively.

$$R_{conv} = \frac{1}{A \cdot h} \quad (11)$$

$$R_{cond} = \frac{t}{A \cdot k} \quad (12)$$

The convective coefficients are determined via Equation (13).

$$h = \frac{Nu \cdot k}{L} \quad (13)$$

The Nusselt number for both the inside of the tank and outside of the tank are solved using correlations for free convection on a vertical surface as given by Equations (14) and (15).

$$Nu = 0.68 + \frac{0.67 \cdot Ra^{1/4}}{\left[1 + \left(\frac{0.491}{\mathrm{Pr}}\right)^{\left(\frac{9}{16}\right)}\right]^{\left(\frac{4}{9}\right)}} \quad (14)$$

$$Ra = \frac{g\beta\left(T_f - T\right) \cdot L^3}{\nu \cdot \alpha} \quad (15)$$

The heat flow through the thermal circuit is defined by Equation (16).

$$Q = \frac{\Delta T}{R_{Tot}} \quad (16)$$

Another thermal circuit is used to solve for the heat transfer from the converter section, through the fin array and into the oil. This circuit is ultimately used to solve for the temperature of the baseplate. The total resistance from the converter to the oil is given by Equations (17) – (20).

$$R_{tot} = \frac{1}{\eta_0 \cdot h \cdot A} \quad (17)$$

$$\eta_0 = 1 - \frac{NA_f}{A_t}\left(1 - \eta_f\right) \quad (18)$$

$$\eta_f = \frac{\tanh mL_c}{mL_c} \quad (19)$$

$$m = \left(\frac{2h}{kt}\right)^{1/2} \quad (20)$$

In addition to the convective heat transfer throughout the system, the radiative heat transfer must also be accounted for. The radiative load entering the tank is determined using data from NASA Surface Meteorology and Solar Energy Tables for the Southeast, tabulated in Table 3, since this is the expected operating region for this particular augmented transformed design [59].

Table 3. NASA solar energy data

Maximum Insolation Incident on a Horizontal Surface	**5.75 kWh/m^2/day**
Maximum Insolation Incident on a Vertical Surface	3.21 kWh/m^2/day
Average Daylight Hours	10.4 hours

The worst case, having the maximum irradiation for the entire span of daylight hours, is considered to ensure that the power routers are able to withstand all possible conditions. Peaks in insolation are not considered in this steady state solution due to the large thermal mass of the system. The incoming radiation is calculated using Equation (21) [60].

$$Q_{rad,in} = \alpha q'' A_s \qquad (21)$$

The heat leaving the tank through radiation to ambient is given by Equation (22) [60].

$$Q_{rad,out} = A_s \sigma \varepsilon \left(T_s^{\,4} - T_{amb}^{\,4} \right) \qquad (22)$$

3.6 Solution Algorithm

The solution for the analytical thermo-fluidic model begins by defining the operating conditions and geometric parameters of the specific thermosiphon-transformer assembly to be described. The heat transfer and pressure calculations developed in the previous section along with a thermodynamic first law energy balance are utilized to

solve for the unknowns tabulated in Table 4. With seven unknowns, seven constraint equations are developed to completely describe steady state operation of the transformer-thermosiphon assembly.

Table 4. Key unknowns in analytical model

Variable	Designator	Units
Fluid temperature at the bottom of the tank	T_1	K
Fluid temperature at the top of the tank	T_2	K
Fluid temperature at the top of the transformer core	T_3	K
Fluid temperature at the top of the upper manifold	T_5	K
Mass flow rate of fluid through the plenum	$\dot{m}_{converter}$	kg/s
Mass flow rate of fluid through the transformer core	$\dot{m}_{transformer}$	kg/s
Temperature of the mounting plate	$T_{baseplate}$	K

The constraints are given by Equations (23) – (28). The constraint described by Equation (23) specifies that the pressure gains must equal the pressure losses around the converter loop.

$$dP_{buoy,conv} - dP_{maj,conv} - dP_{\min or,conv} + dP_{buoy,TX} - dP_{maj,TX} = 0 \qquad (23)$$

The constraint described by Equation (24) specifies that the pressure gains must equal the pressure losses around the transformer core loop.

$$dP_{buoy,CTX} - dP_{maj,CTX} - dP_{\min or,CTX} + dP_{buoy,TX} - dP_{maj,TX} = 0 \qquad (24)$$

The constraint described by Equation (25) is a utilization of the conservation of energy principle and specifies that the heat entering temperature node 2 must equal the heat leaving the same node.

$$\dot{m}_{conv} \cdot c_p \cdot (T_5 - T_2) + \dot{m}_{TX} \cdot c_p \cdot (T_3 - T_2) = 0 \qquad (25)$$

The constraints described by Equations (26) and (27) utilize the first law to specify that the heat entering a section must be equal to the change in internal energy across that section.

$$Q_c - \dot{m}_{conv} \cdot c_p \cdot (T_5 - T_1) = 0 \quad (26)$$

$$Q_{TX} - \dot{m}_{TX} \cdot c_p \cdot (T_3 - T_1) = 0 \quad (27)$$

The constraint described by Equation (28) utilizes the first law to specify that the total heat into the system must be equal to the total heat leaving the system.

$$Q_c + Q_{TX} + Q_{rad,in} - Q_{conv,out} - Q_{rad,out} = 0 \quad (28)$$

The temperature of the baseplate is the ultimate metric for successful operation of the system. With the oil temperatures and mass flow rates known, the temperature of the baseplate can be calculated. The constraint described by Equation (28) utilizes a heat transfer analysis to determine the temperature of the baseplate from the amount of heat added from the converter, the temperature of the fluid and the thermal resistance from the fluid to the baseplate.

$$Q_c - \frac{T_{baseplate} - T_{fluid}}{R_{tot}} = 0 \quad (29)$$

3.7 Analytical model results

The inputs for this model, tabulated in Table 5 are determined from a prototype converter that utilizes existing transformer technology. The model was implemented in Engineering Equation Solver (EES) v9.452 using the boundary conditions and specified design inputs presented in Table 4. EES is an equation solving program that can rapidly solve thousands of coupled non-linear algebraic and differential equations.

Table 5. Inputs to the model

Heat from converter	**80 W**
Heat from Transformer Core	700 W
Height of the Plenum	0.31785 m
Width of the Plenum	0.3175 m
Depth of the Plenum	0.06096 m
Height of Transformer Tank	1.016 m
Diameter of Transformer Tank	0.508 m
Height of Transformer Core	0.8636 m
Diameter of Transformer Core	0.05398 m
Height of Lower Manifold	0.3767 m
Diameter of Lower Manifold	0.0409 m
Height of Upper Manifold	0.3767 m
Diameter of Upper Manifold	0.0409 m
Number of Fins in Fin Array	26
Spacing Between Fins	0.005 m
Height of Fins	0.04 m
Width of Fins	0.004 m

EES solves for all unknowns and parametric tables are used to solve for various ambient temperatures and converter loads. The model outputs four oil temperatures, the mass flow rates of oil through the transformer core and converter, and the temperature of the mounting plate. The temperature of the baseplate with varying converter loads and ambient temperatures with no irradiation is shown in Figure 19. The maximum junction temperature for the converter device packages is 125 °C meaning that the baseplate must be kept below 104 °C. The maximum ambient temperature that the devices must withstand is 40 °C. With no irradiation, the baseplate temperatures are safely below the maximum baseplate temperature.

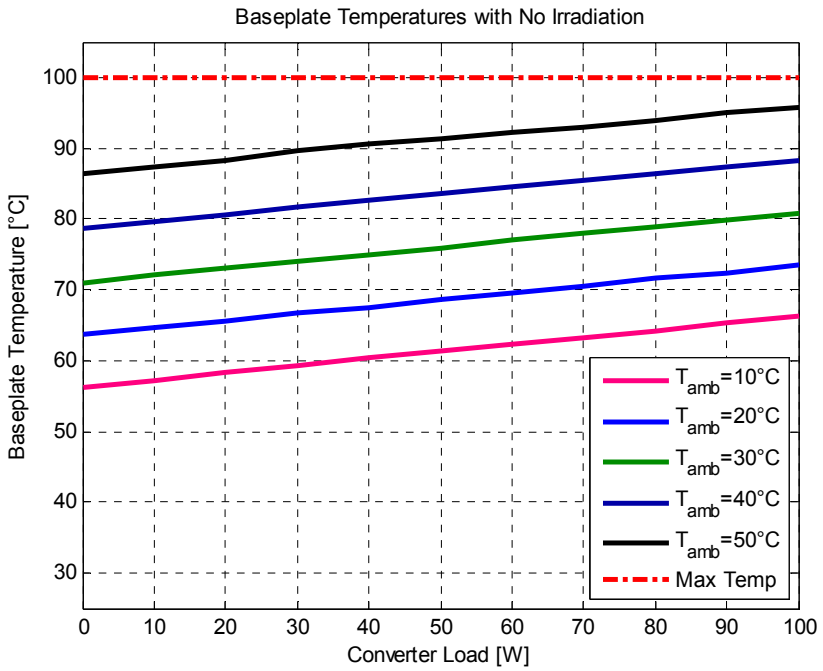

Figure 19. Results from analytical model showing baseplate temperatures at various converter loads and ambient temperatures with no irradiation

The results for solving the analytical model at a converter load of 80 W and various ambient temperatures are tabulated in Table 6.

Table 6. Results from analytical model at 80 W converter load and various ambient temperatures with no irradiation

T_{amb}	10°C	20°C	30°C	40°C	50°C
$T_{baseplate}$ (°C)	64.3	71.5	78.9	86.3	94
T_1 (°C)	60.2	67.3	74.6	82.1	89.6
T_2 (°C)	63.2	70.4	77.7	85.1	92.7
T_3 (°C)	66.3	73.5	80.8	88.2	95.8
T_5 (°C)	60.7	67.9	75.2	82.6	90.2
$\dot{m}_{converter}$ (kg/s)	0.0816	0.0816	0.0816	0.0816	0.0816
$\dot{m}_{transformer}$ (kg/s)	0.052	0.052	0.052	0.052	0.052

The low mass flow rates confirm the laminar flow assumption made for the pressure and heat transfer correlations in the model development. The temperature of the mounting plate with varying converter loads and ambient temperatures with the irradiation experienced on a sunny day in the Southeast is shown in Figure 20. An emissivity of 0.28 and an absorptivity of 0.8 were used as these are the values for uncoated sheet metal [60].

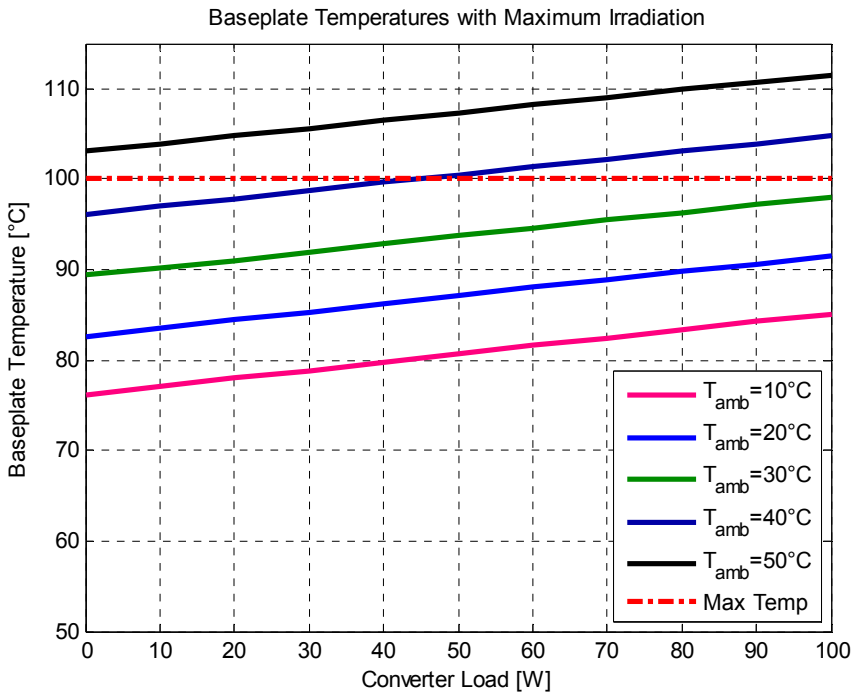

Figure 20. Results from analytical model showing baseplate temperatures at various converter loads and ambient temperatures with maximum irradiation experienced in Southeast

With this radiative load, the temperature of the baseplate exceeds the maximum baseplate temperature at all converter loads greater than 45W at an ambient temperature of 40 °C and exceeds the maximum baseplate temperature for all converter loads at an ambient

temperature of 50 °C. In order to keep the baseplate at an operable temperature, a coating needs to be added to the outside of the transformer to reduce the incoming irradiation. The emissivity and absorptivity for different surface coatins is tabulated in Table 7 [61].

Table 7. Emissivity and absorptivity values for different surface coatings

Surface Coating	Emissivity	Absorbtivity
White Lead Paint	0.9	0.25
Light Cream Paint	0.9	0.35
Aluminum Paint	0.55	0.55
Gray Paint	0.9	0.75
Mat Black Paint	0.95	0.97

Baseplate temperatures with varying surface coatings on the transformer with a 40 °C ambient temperature are shown in Figure 21.

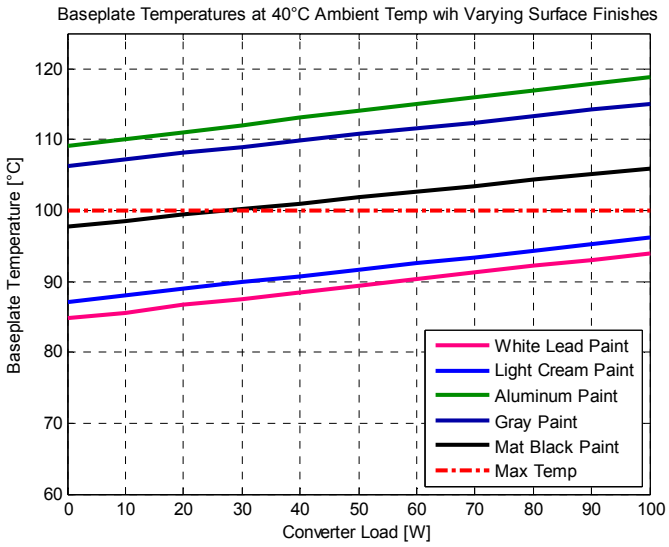

Figure 21. Results from analytical model showing baseplate temperatures at various converter loads at an ambient temperature of 40 °C with maximum irradiation experienced in Southeast and varying surface finishes

The transformer must be coated with either a white lead paint or light cream paint in order to keep the mounting plate at an operable temperature. It could also be coated with a paint that has either the same or higher emissivity and the same or lower absorptivity than the recommended options. The results for solving the analytical model at a converter load of 80 W, ambient temperature of 40 °C, and various surface finishes are tabulated in Table 8.

Table 8**.** Results from analytical model at 80 W converter load, an ambient temperature of 40 °C and various surface finishes

Surface Coating	**White Lead Paint**	**Light Creme Paint**	**Aluminum Paint**	**Gray Paint**	**Mat Black Paint**
T_1 (°C)	87.8	90	112.9	98.9	101.4
T_2 (°C)	88.1	90.4	113.3	99.2	101.7
T_3 (°C)	88.1	90.4	113.3	99.2	101.7
T_5 (°C)	88.7	91	113.8	99.8	102.3
$\dot{m}_{converter}$ (kg/s)	0.0472	0.0472	0.0472	0.0472	0.0472
$\dot{m}_{transformer}$ (kg/s)	1.073	1.073	1.073	1.073	1.073

This study shows the importance of considering the irradiation when designing thermal management devices for use in ambient conditions exposed to direct sunlight. The coating on the surface of the thermosiphon-transformer assembly causes up to a 25°C difference in temperatures.

3.8 50 kVA thermosiphon construction

The thermosiphon was built in MayorLab and then shipped to T&R Electric to be welded onto a 50 kVA transformer. The list of materials for the thermosiphon is tabulated in Table 9.

Table 9. Bill of materials for thermosiphon construction

Line	Product	Unit Price	Quantity	Total
1	Sheet steel, 0.075" thick, 24"x36"	$64.95	1	$64.95
2	Aluminum, 1/4" thick, 24"x24"	$153.91	2	$307.82
3	Steel 1-1/2 Pipe, 5' length	$56.12	2	$112.24
4	Wall Butt-Weld Steel, 90 degree Elbow	$12.56	8	$100.48
5	Steel bar, 1/8" thick, 2-1/2" width, 2' length	$10.20	1	$10.20
6	Aavid fin array, 65615, W=9.03", length 7.4'	$762.50	1	$762.50
7	Hardware	10% of total		$64.95
Total				$747.00

The sheet metal and aluminum plate profile were cut with a Maxiem 1515 waterjet which has a tolerance of ±0.003”. The welding process for the 50 kVA thermosiphon is depicted in Figure 22. The top left picture depicts the TIG welding of the plenum, which was welded on both sides to ensure that no leaks would form. The bottom left picture depicts the weld on the corner of the plenum and the straight pipe which had been tacked into place. The top right picture depicts the weld from the straight pipes to the 90° bends. The bottom right picture depicts the thermosiphon assembly prior to fully welding the straight pipes into the plenum. As is depicted, the pipes were all tacked into place to ensure alignment before fully welding.

Figure 22. Pictures from the Welding Process for the 50 kVA Thermosiphon

The sheet metal for the plenum was bent into the proper configuration using a magnetic bender prior to welding. Once the plenum welding was completed, the straight pipes were welded onto the plenum, and lastly the 90° bends were welded onto the straight pipes. The fully welded thermosiphon assembly is depicted in Figure 23.

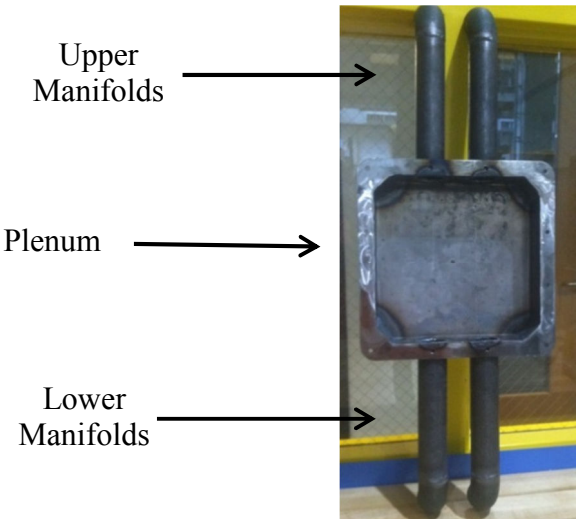

Figure 23: 50 kVA Thermosiphon after welding

After welding was completed, the assembly was primed and painted. The mounting plate holes and groove for a foam gasket were machined on a 3-axis CNC mill (Prototrak DPM SX2). Before shipping, the thermosiphon was assembled and tested for leaks. The final assembly is depicted in Figure 24.

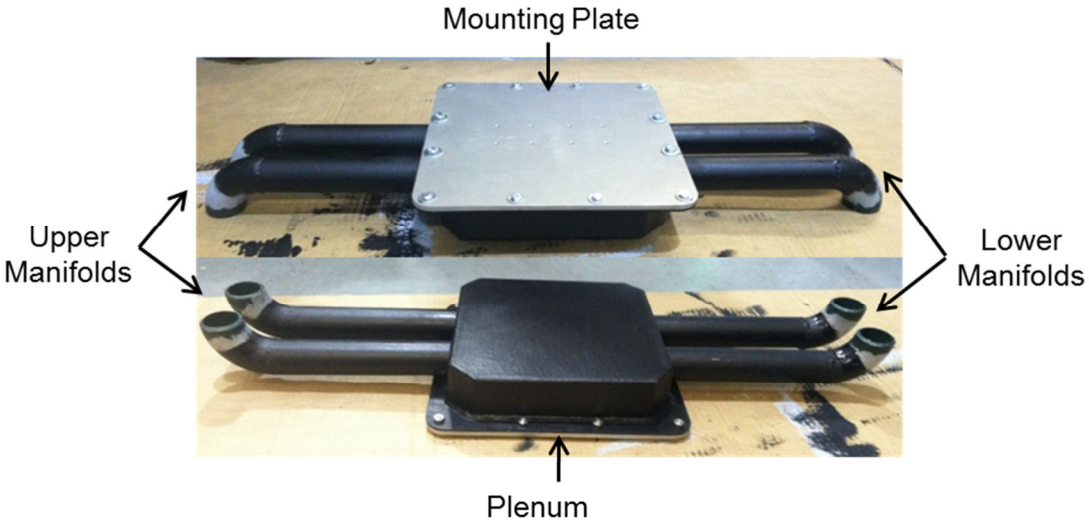

Figure 24: Final 50 kVA Thermosiphon Assembly

Copper heater blocks were machined to match the solid state device footprint. Cartridge heaters were inserted into slots machined in the copper blocks with thermal paste. The heater blocks with cartridge heaters were then potted in thermally insulating epoxy to ensure at least 97% of the thermal load travelled through the copper block and into the mounting plate. The thermal load from the copper heater blocks was controlled by a variac. The final construction was shipped to T&R Transformers to be welded onto the transformer. The completed assembly without the heater blocks, depicted in Figure 25, was shipped to the National Electric Energy Testing Research and Applications Center (NEETRAC) where the experimental tests were performed.

Figure 25: Final Thermosiphon-Transformer Assembly

3.9 50 kVA thermosiphon-transformer testing

The 50 kVA transformer was tested at its maximum operating temperature of 40°C and at room temperature. The test setup is depicted in Figure 26. An elevated ambient testing chamber, as developed by Loeffler, was used to control the ambient temperature experienced by the transformer. The chamber is an 8’ cube consisting of 9 panels constructed of 2”x2” frame supporting ¼”x4’x8’ sheets of plywood along with foam insulation board that was glued to the inside of the panels to reduce heat loss through the walls. The door of the test chamber was constructed of plexi-glass to allow access as well as viewing for early detection of any problems during the testing. Two DC fans, built into one wall, were utilized for flow rate control through the chamber. A wall of honeycomb, located between the test section and the fans, created laminar air flow into the test section. Insulation board was used to cover the concrete floor of the test section because the concrete acts as a heat sink making the elevated temperature increasingly difficult to

maintain without the insulation. Portable heaters were used to preheat the testing chamber up to the required 40 °C.

Figure 26: 50 kVA thermosiphon-transformer assembly in testing chamber

A digital proportional-derivative-integral (PID) control was used to the control the voltage to the fans and therefore the temperature within the chamber. A T-type thermocouple was used to measure the ambient temperature within the chamber, which is the input to the PID controller. The PID controller calculates the error as the difference between the measured ambient temperature and the desired set point temperature. The PID controller utilizes the values for the proportional, derivative and integral gain to adjust the output, in this case the voltage to the fans, to minimize this error. Mounting plate temperatures were measured using surface thermocouples and fluid temperatures were measured using T-type thermocouples. These temperatures were collected and

stored using a 16 channel thermocouple DAQ card. The apparatus and their associated uncertainties for the experiment are tabulated in Table 10.

Table 10: Apparatus with associated uncertainty

Measurement Apparatus	Model	Uncertainty
Digital Voltmeter	Fluke 179	1.0% + 3 counts
Digital Ohmmeter	Fluke 179	0.9% + 1 count
Surface Thermocouple	Omega T-type	1.0 °C
Thermocouple	Omega T-type	1.0 °C
Variac	Staco 3PN1010	N/A
16 Ch. Thermocouple DAQ	NI 9213	N/A

Eight individual tests were performed at different ambient temperatures and load cases, the results of which are tabulated in Table 11.

Table 11. Results from 50 kVA testing

Test Number	Test Duration (hrs)	Transformer Load (W)	Converter Load (W)	Ambient Temperature (°C)	Maximum Baseplate Temperature (°C)
1	2.75	700	80	uncontrolled	48.7
2	8.75	700	80	24	65.3
3	9.75	700	80	40	75.2
4	9.75	700	80	40	75.5
5	9.75	560	80	40	63.4
6	12	700	0	40	76.8
7	15	700	80	40	81.3
8	14.75	700	80	24.5	66.2

The data from the table shows that the mounting plate was safely below the maximum temperature of 104°C for all trials. The last two trials were further analyzed since they ran longest and temperatures were close to steady state. The results from these tests were used to validate the analytical model. The buoyant flow through the thermosiphon begins approximately 0.5 hour into test 7, as shown the testing temperatures in Figure 27. The ripples in the ambient temperature were due to the air conditioning cycling on in the

testing facility and the system response to the change. Even with these ripples, the ambient temperature stayed within 1 °C of the desired 40 ° ambient for the duration of the test once it was reached about 1.5 hours into the test.

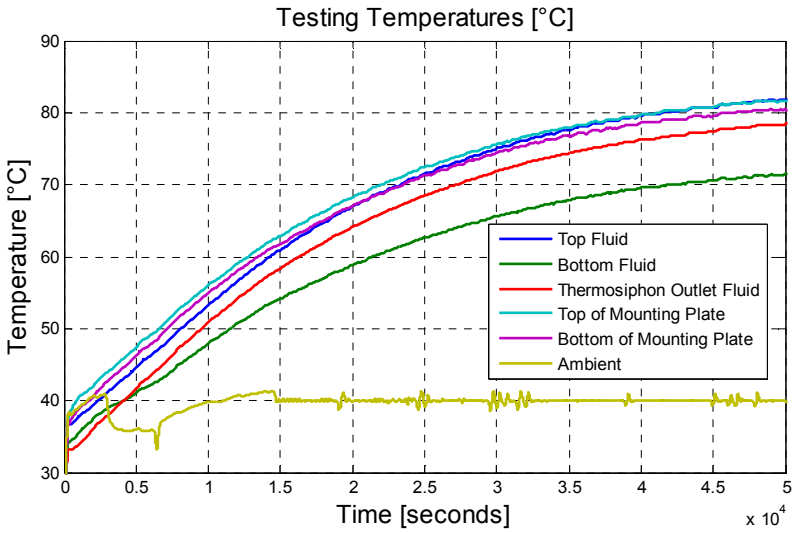

Figure 27. Mounting Plate and Fluid Temperatures and Ambient Temperature at Full Transformer Load and Full Converter Load with an ambient temperature maintained at 40°C

The last hour of testing temperatures, as shown in Figure 28, shows that the temperatures were still changing as much as 1.5°C over the hour.

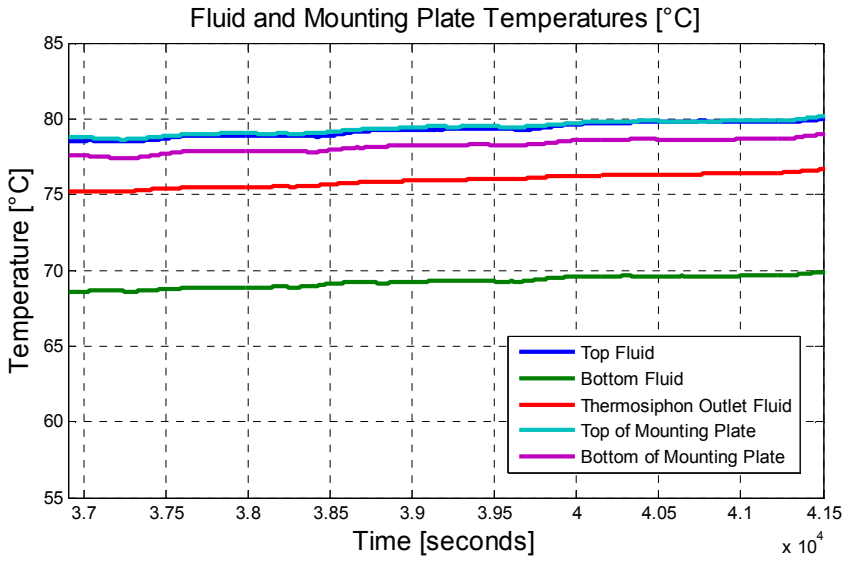

Figure 28. System temperatures for the last hour of testing at full transformer and converter load and an ambient temperature of 40°C

The ambient temperature for the last hour of testing, as shown in Figure 29, shows that the increase in system temperatures was not due to an increase in ambient temperatures.

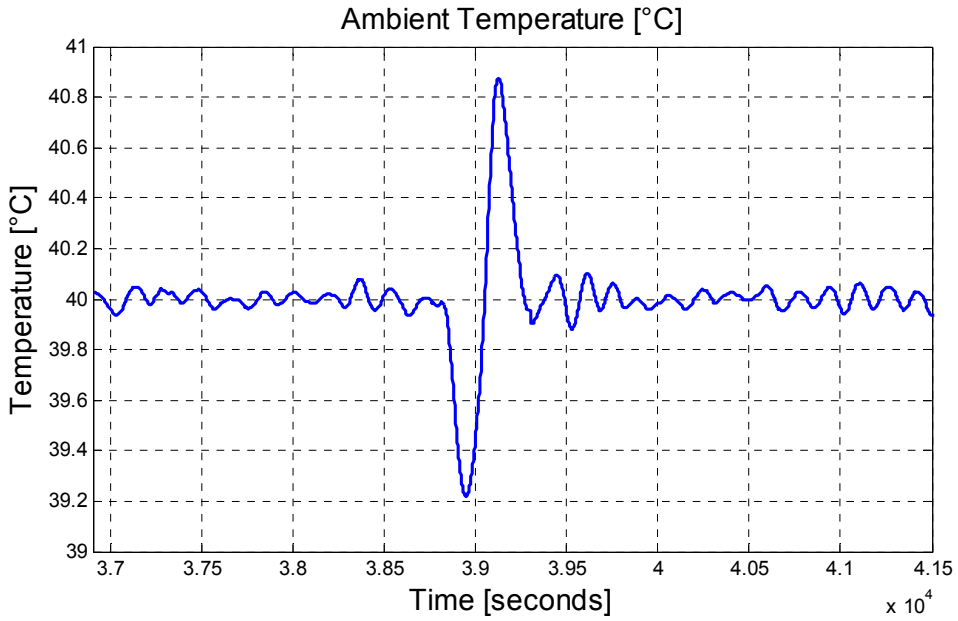

Figure 29. Ambient temperature control for the last hour of testing in test 7 at full transformer and converter load

The ambient temperature stayed within 1°C of the desired temperature as seen in the ambient temperature plot. When the air conditioning at the testing facility turned on, there was a large drop in the temperature of the incoming air to the chamber causing the dip in the plots. This dip is followed by a spike which is the system response to the colder inlet air.

Since the temperature of the system was still changing by 1°C every hour, a plot was created to show the change in temperature over the change in time. As the system approaches steady state, the change in temperature should trend to zero. This trend is shown in Figure 30 and shows the Dt/dt plot for test 7. The change in temperature for all fluid temperatures and mounting plate temperatures decreases as the test progresses, but none of the temperatures except for the ambient temperature cross zero. This would suggest that the trial did not quite reach steady state.

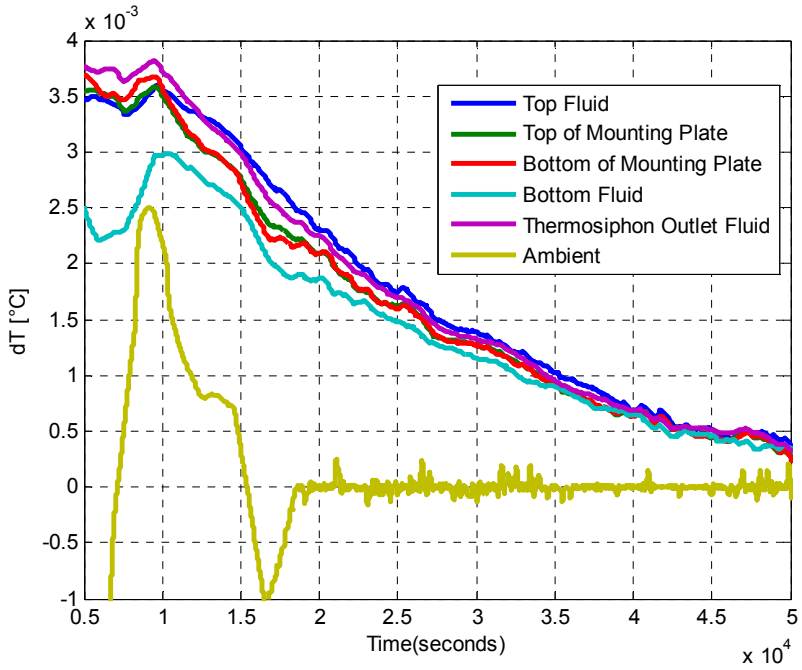

Figure 30. Derivative of the Change in Temperature over the Duration of the Test at full transformer and converter load and ambient temperature of 40°C

Since steady state was not achieved during testing, the temperature data for the fluid and mounting plate was fit to curves using the Matlab fit function using Equation (29), as shown in Figure 31. The plot shows the data, the extrapolated curve and the 95% confidence bounds around the extrapolated curve. The fit function in Matlab uses a nonlinear least squares method to minimize the error.

$$T = e^{-at} \cdot \left(T_{\inf} - T_i - \left(\frac{b}{a} \right) \right) + T_{\inf} + \left(\frac{b}{a} \right) \quad (29)$$

The use of the equation defined by the lumped capacitance method is utilized by treating the thermocouple as a small solid body surrounded by the fluid. The heat dissipated by the transformer and converter into the oil is considered constant. In this respect, a constant heat source is added to the fluid and therefore added to the thermocouple. Because the Biot number of the thermocouple, given by Equation (29), is around 1.4 x 10^{-4} , conservatively assuming that h = 7 W/m^{2}K, d = .51 mm and k = 25 W/mK, the lumped capacitance method is valid and the thermocouple temperature can be regarded as uniform throughout the bead.

$$Bi = \frac{hD}{k} \quad (30)$$

The time constant of the system is found by utilizing Equation (31).

$$\tau = \frac{1}{a} \quad (31)$$

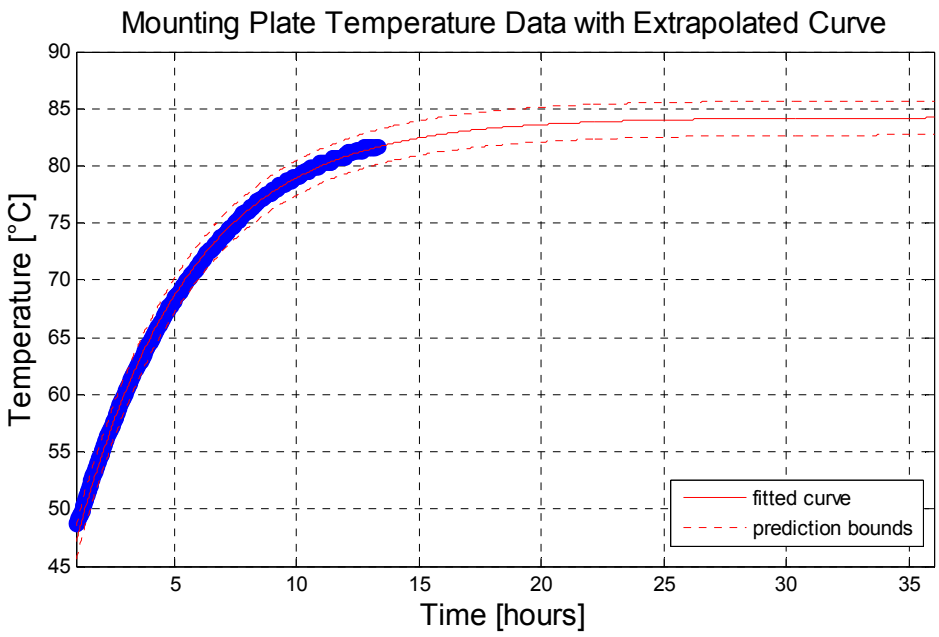

Figure 31. Curve Fit to Temperature Data for the Mounting Plate with Full Transformer and Converter Load with an Ambient Temperature of 40°C

The R^2 for this fit is 99.54%, further validating the use of the lumped capacitance equation for the fit. The curves for all temperatures were extrapolated, as shown in Figure 32, to show the steady state temperatures of the system.

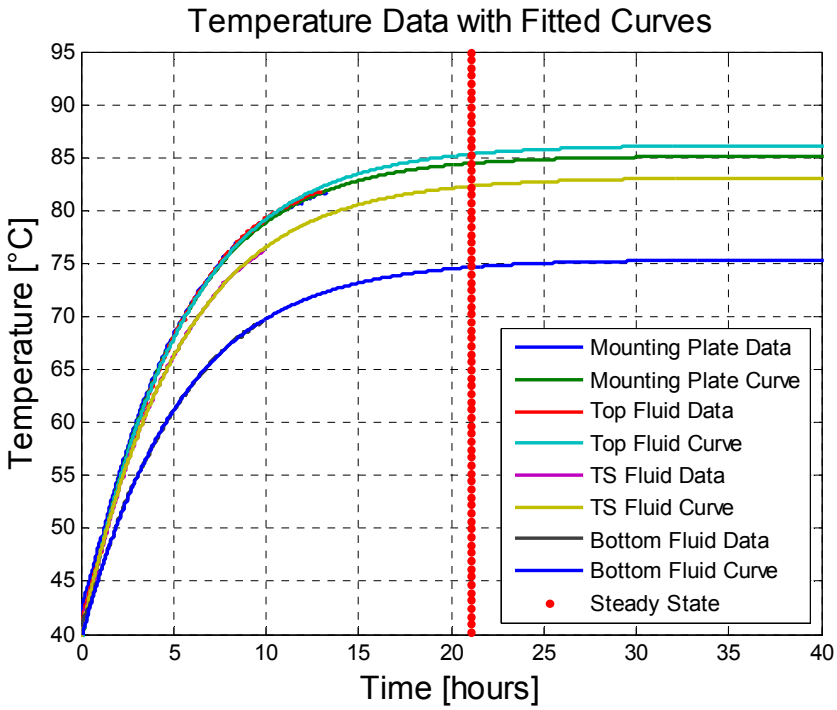

Figure 32. Curves Fit to Temperature Data for Top Fluid with Full Transformer and Converter Load with an Ambient Temperature of 40 °C

The time constant as defined by the curve is 5.262 hours. Steady state is described as 4 times the time constant giving a total testing time of 21.048 hours to reach steady state, which is shown as a red dotted line in the plot. Due to the high voltage nature of the test and testing requirements by NEETRAC, the test was not allowed to run for more than 15 hours and therefore this is the longest the test could run.

The same analysis was repeated for test 8 to provide an additional operating condition for validation of the analytical model. The results for test 8 with an ambient temperature of 24.5 °C, plotted in Figure 33, show the baseplate temperatures are again safely under the maximum operating conditions. The onset of buoyant flow through the

thermosiphon is seen as the temperature difference between the thermosiphon outlet and fluid at the bottom of the tank starts to increase about 0.5 hours into testing.

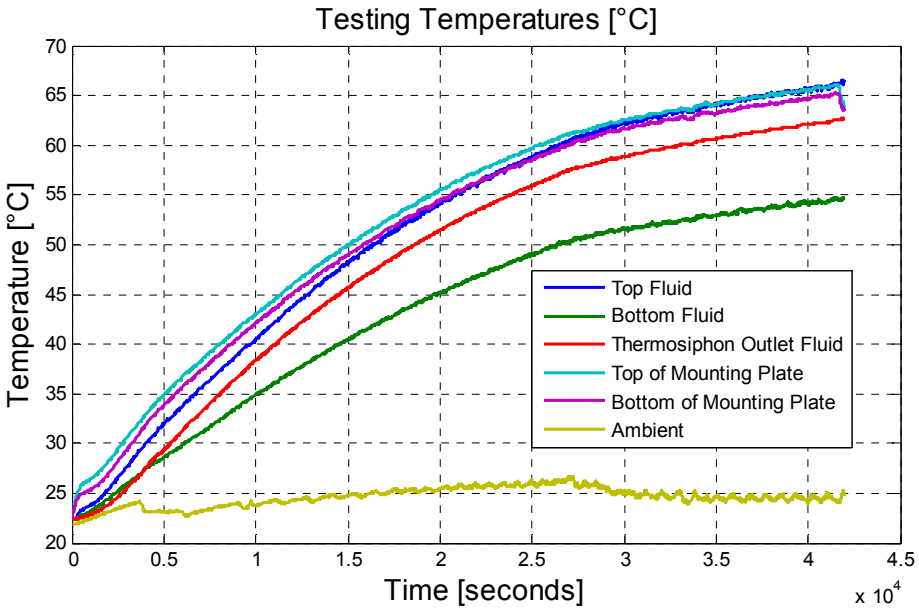

Figure 33. Mounting Plate and Fluid Temperatures and Ambient Temperature at Full Transformer Load and Full Converter Load with an ambient temperature maintained at 24.5°C

The last hour of testing temperatures, as shown in Figure 34, shows that the temperatures were still changing as much as 1°C over the hour and the system had not achieved steady state.

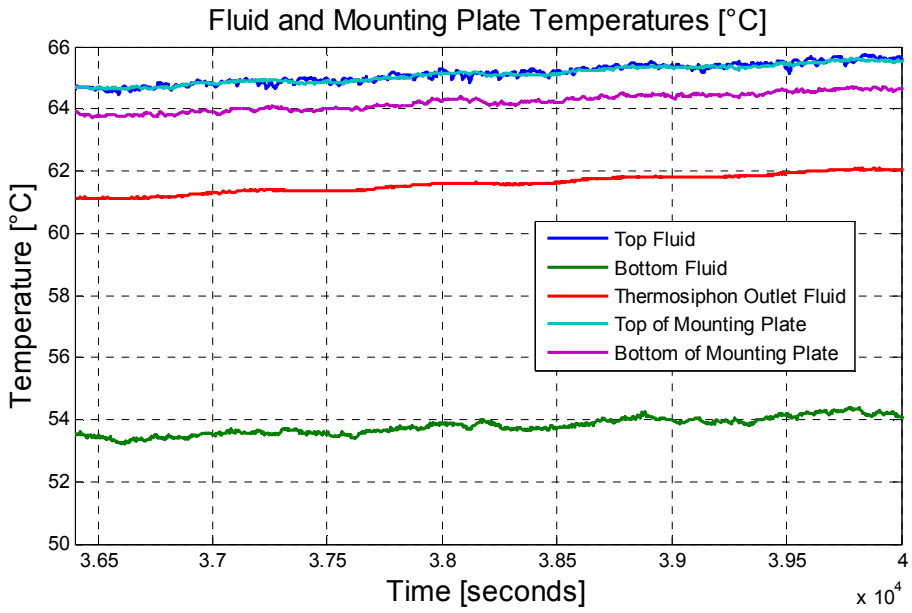

Figure 34. System temperatures for the last hour of testing during test 8 at full transformer and converter load and an ambient temperature of 24.5°C

The ambient temperature for the last hour of testing, as shown inFigure 29, shows that the increase in system temperatures was not due to an increase in ambient temperatures. The temperature for this trial stayed within 0.5°C of the desired temperature, and there are no drastic dips and recoveries during this run due to more favorable weather conditions reducing the need for air conditioning in the testing facility.

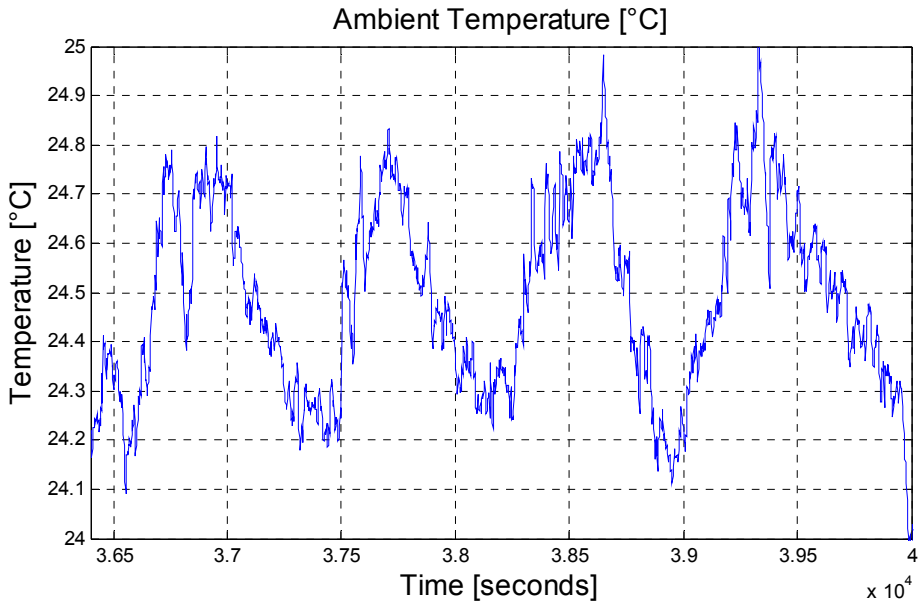

Figure 35. Ambient temperature control for the last hour of testing during test 8 at full transformer and converter load

The dT/dt plot for test 8 is shown in Figure 36. The change in temperature for all fluid temperatures and mounting plate temperatures decreases as the test progresses, but none of the temperatures except for the ambient temperature cross zero. This would again suggest that the trial did not quite reach steady state.

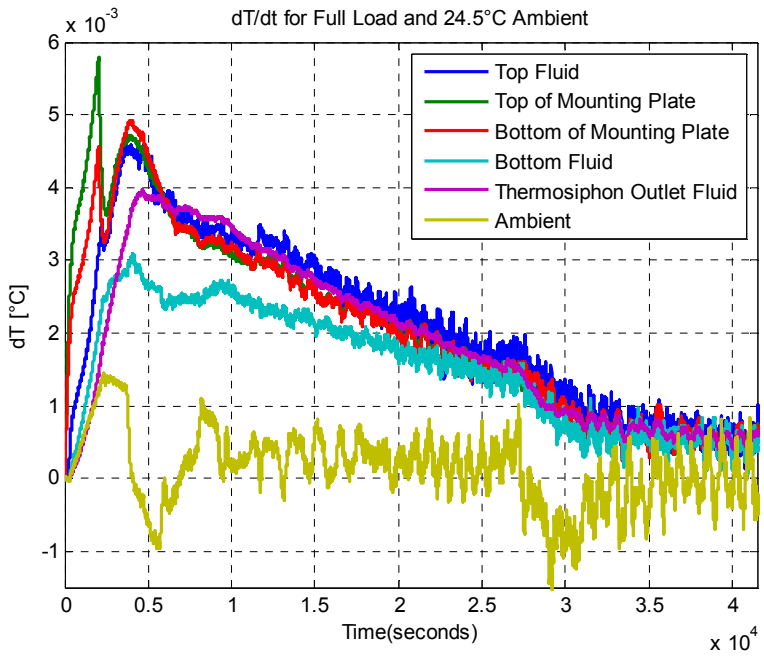

Figure 36. Derivative of the Change in Temperature over the Duration of Test 8 at full transformer and converter load and ambient temperature of 24.5°C

Again the steady state was not achieved during the test due to the safety policy of the testing facility that prohibits operation of high voltage devices overnight. The temperature data for the fluid and mounting plate was fit to curves using the MATLAB fit function and Equation (29), as shown in Figure 37. The plot shows the data, the extrapolated curve and the 95% confidence bounds around the extrapolated curve.

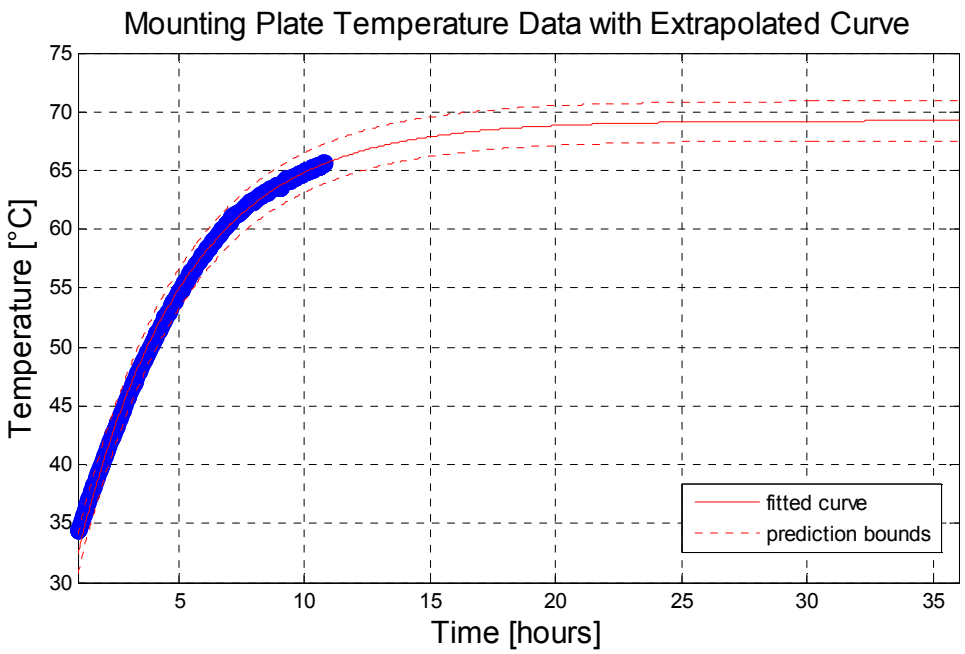

Figure 37. Curve Fit to Temperature Data for Top Fluid with Full Transformer and Converter Load with an Ambient Temperature of 24.5°C

The R^2 for this fit is 99.16%, showing again that using the lumped capacitance equation for the fit is a valid assumption. The curves for all temperatures were extrapolated, as shown in Figure 32, to show the steady state temperatures of the system.

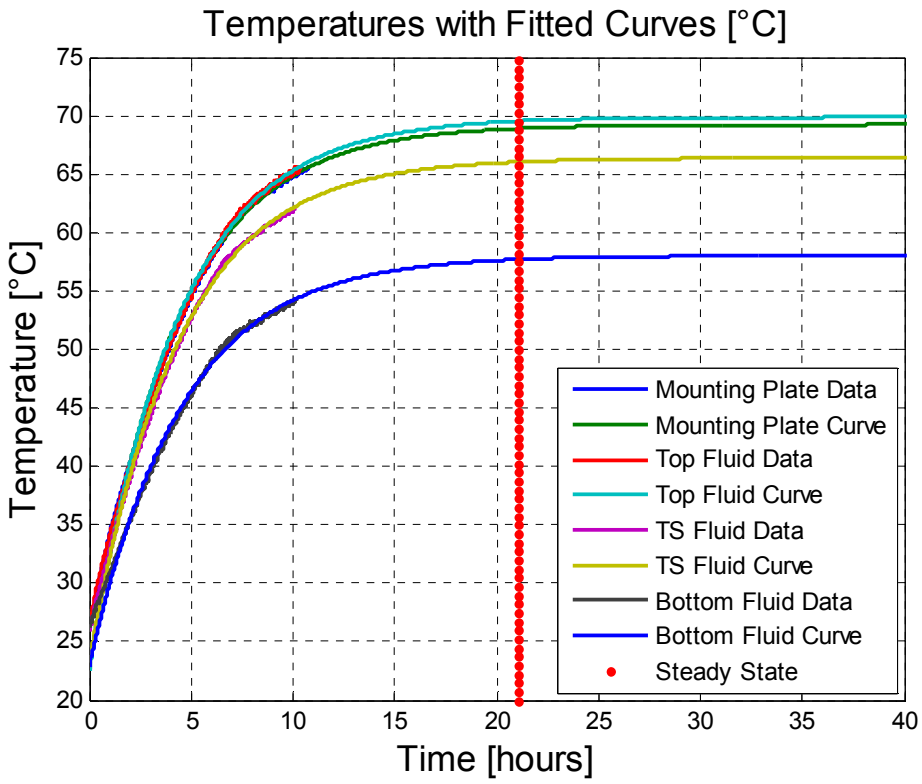

Figure 38. Curves Fit to Temperature Data for Top Fluid with Full Transformer and Converter Load with an Ambient Temperature of 24.5°C

The time constant for the system was determined to be 5.261 hours, giving a total testing time of 21.044 hours to reach steady state. The steady state temperatures described by the curve fits from the experimental data were compared to the steady state temperatures given by the analytical model as tabulated in Table 12.

Table 12. Analytical EES steady state temperatures compared to Experimental Steady state temperatures tested at full transformer and full converter loads

Test	Ambient Temp	Description	Mounting Plate	Core Exit	Thermosiphon Exit	Bottom Fluid
7	40	Experimental	86.16	85.14	83.1	75.35
		Model Prediction	85.1	83.6	83.6	78.5
		Difference	**1.06**	**1.54**	**0.5**	**3.15**
8	24.5	Experimental	69.86	73.05	69.21	58.51
		Model Prediction	69.9	71.45	69.45	63.35
		Difference	**0.04**	**1.6**	**0.24**	**4.84**

Maximum disagreement between the model and experimental data was 1.06°C for the mounting plate temperature and 4.84°C for the fluid temperatures.

3.10 Uncertainty Analysis

Equipment measurement uncertainties were considered to determine the total experimental uncertainty for the data. Kline and McClintock's method for single measurement uncertainty was used to calculate the total uncertainty for the collected data. The individual measurements and associated uncertainties are presented in Table 13 and Table 14.

Table 13. Measurements and associated uncertainties for power calculation

Voltage [V]	σV [V]	Resistance [Ohms]	σR [Ohms]	Power [W]	σP [W]
77.1	3.77	74.2	1.67	80.11	8.04
76.7	3.77	73.5	1.66	80.04	8.07

Table 14. Measurements and uncertainty for thermal resistance calculation

Power [W]	σP [W]	$T_{mounting}$ [°C]	T_{amb} [°C]	ΔT [°C]	σΔT [°C]	$R_{Thermal}$ [°C/W]	$\sigma R_{Thermal}$ [°C/W]
80.11	8.04	86.16	40	46.16	1.41	0.5762	0.0605
80.04	8.07	69.86	25	45.36	1.41	0.5667	0.0598

The primary contributor to the uncertainty in the data is the power measurement due to the voltage being squared in the power formula. The model was evaluated at both ambient temperatures that were tested. The values for the experimental and model mounting temperatures and thermal resistance are compared and tabulated in Table 15.

Table 15. Comparison of model predictions against experimental values

Power [W]	T_{amb} [°C]	$T_{mount, exp}$ [°C]	$T_{mount, model}$ [°C]	ΔT [°C]	$R_{Therm, exp}$ [°C/W]	$R_{Therm, model}$ [°C/W]	R_{Therm} Error [%]
80.11	40	86.16	85.1	1.06	0.5762	0.5630	2.35
80.04	25	69.86	69.9	0.04	0.5667	0.5672	0.09

The mounting plate measurement, at an ambient temperature of 24.5 °C, falls within the experimental uncertainty of the thermocouple readings. At an ambient temperature of 40°C the mounting plate temperature differs from the model predictions by more than the experimental uncertainty of 1°C by only 0.06 °C. The maximum disagreement between the model and experimental thermal resistance was 2.35% which is within the given experimental uncertainty.

3.11 Summary

An analytic thermo-fluidic model for a 50 kVA dual-loop single phase thermosiphon-transformer assembly is presented. The thermosiphon-transformer assembly is constructed and tested experimentally at two different ambient temperatures to compare experimental results to the model results. The maximum disagreement between the model and experimental data was 1.06 °C for the mounting plate temperatures and 2.35% for the thermal resistance. The code solves in less than 0.1 seconds and accurately predicts the performance of a given thermosiphon-transformer assembly.

CHAPTER 4

1 MVA DUAL LOOP THERMOSIPHON-TRANSFORMER ASSEMBLY

4.1 Introduction

This chapter presents a single-phase thermosiphon coupled to a 1 MVA transformer for power electronics cooling. This assembly will build upon the model developed for the 50 kVA model to prove the concept prior to the build and experimentation. The 1 MVA thermosiphon-transformer assembly includes a secondary-loop cooling path that utilizes the cooling oil already present in the transformer to also cool the converter. The primary differences between the assembly for the 50 kVA transformer and the assembly for the 1 MVA transformer are that the 1 MVA transformer is three phase so will utilize three power converters all with individual thermosiphons and radiators are added on to the transformer due to the increased thermal load. The additional heat input from the 1 MVA transformer with the three power converters makes the addition of radiators necessary to increase the area for rejection heat to the ambient. The 1 MVA analytical model will again seek to create a description of the steady state operation of a specific dual-loop thermosiphon design. This specific thermosiphon design is then manufactured and tested. The experimental mounting plate temperatures are then compared to the theoretical mounting plate temperatures predicted by the model.

4.2 1 MVA Thermosiphon-Transformer Assembly Design

The incorporation of the thermosiphon into the transformer utilized design specifications and constraints from the converter manufacturer and transformer manufacturer. The compiled list of specifications and constraints for the transformer and converter are tabulated in Table 16.

Table 16. 1 MVA converter and transformer specifications

Specification	Unit	Value
Nominal Power (rated)	MW	1
Nom. Converter Loss	W	2100
Nom. thermal loss per device	W	300
Max. switch junction temperature	C	125
Thermal resistance, junction to baseplate IGBT	K/W	0.038
Thermal resistance, junction to baseplate Diode	K/W	0.068
Max. mass of converter (incl. cold plate) per phase	lbs	150
Max. height of cold plate	in	28
Max. width of cold plate	in	13
Max. depth of converter	in	12
Ambient temperature	C	40
Target climate of test site	N/A	South East
Max. width of pad	ft	10
Max. length of pad	ft	10
Max. height of enclosure	ft	6
Target height of enclosure	ft	5
Enclosure protection rating (NEMA)	NEMA	3R
Enclosure protection rating (IP)	IP	14
Max. width of enclosure	ft	8
Max. length (breadth) of enclosure	ft	8
3-phase transformer losses	W	12388
Transformer cabinet width	in	70
Transformer tank width	in	66
Transformer depth (overall)	in	65
Transformer depth (cabinet)	in	18
Transformer depth (tank)	in	30
Thickness of sheet metal for tank	in	0.25
Transformer height	in	53
Volume of oil in Transformer	gal.	340
Height of oil in Transformer	in	41
Transformer Core Width	in	52
Transformer Core depth with windings	in	22.4
Transformer Core max Height	in	34
Transformer Core Window Height	in	14
Transformer Core Sheet Width	in	9.75
Transformer Core Window Width – wide	in	8
Transformer Core Window Width – narrow	in	4
Transformer Core to ground Distance	in	3/8 - ½

Several preliminary design configurations were developed and are depicted in Figure 39. Configuration 1 contains oil filled fins along the back of the transformer with two converters mounted on one side and one converter mounted on the opposite side. The next configuration requires all three of the converters mounted along the back side and an equal number of radiators on each side of the transformer tank. The third design possibility requires the three converters stacked horizontally on one side of the transformer tank, oil filled plates along the back of the transformer tank and radiators on the opposite side of the tank as the converters. The fourth design proposes unique offset manifolds that allow all three converters to be mounted vertically on one side of the tank with oil filled plates along the back of the tank and additional radiators on the other side of the tank. The fifth configuration is similar to the fourth except the manifold extends from the transformer at one location and branches out to provide oil to the three converters. The final proposed configuration presents the converters in a separate assembly from the transformer with each converter utilizing its own radiator.

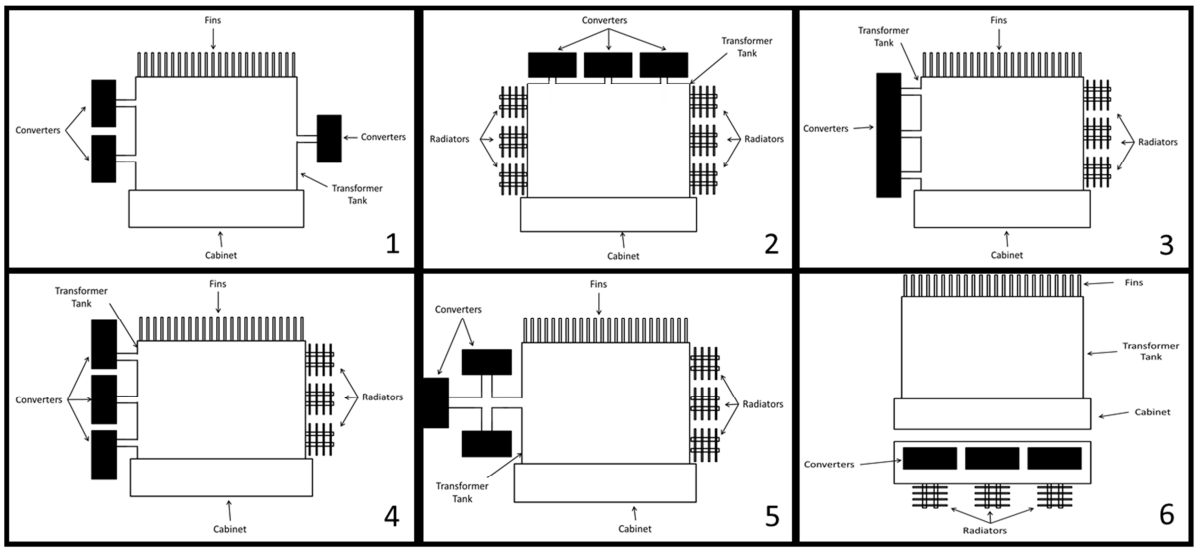

Figure 39. Possible configurations for 1 MVA thermosiphon-transformer assembly

Each design was evaluated based on four criteria: ability to effectively cool the converters, ability to uniformly cool the converters, manufacturing complexity and cost. Each of these design criteria was assigned a weight and each configuration was rated from 0-10 based on the design criteria. The results were tabulated into a weighted evaluation matrix, Table 17, to determine the optimal design configuration.

Table 17. Weighted evaluation matrix

Criteria	Weight	Option 1		Option 2		Option 3		Option 4		Option 5		Option 6	
Effective Cooling	35	6	2.1	7	2.45	9	3.15	9	3.15	8	2.8	9	3.15
Uniform Cooling	25	2	0.5	8	2	2	0.5	7	1.75	5	1.25	10	2.5
Manufacturability	15	8	1.2	8	1.2	6	0.9	6	0.9	4	0.6	6	0.9
Cost	25	8	2	8	2	7	1.75	7	1.75	6	1.5	2	0.5
Total	**100**	**5.8**		**7.65**		**6.3**		**7.55**		**6.15**		**7.05**	

Option 2, was selected as the optimal configuration for the 1 MVA thermosiphon-transformer assembly. The required cooling capabilities for the radiators were then calculated by first determining the current cooling capability of the transformer. The transformer without the converters utilized four radiator banks each comprised of seven oil filled plates to reject the thermal load from the transformer coils. The heat dissipated from the radiators was calculated using Incropera and DeWitt's correlation for flow between parallel isothermal plates [62, 63]. The cooling capability required to also reject the additional thermal load from the three converters was then calculated. It was determined that eleven oil filled plates would be needed per radiator bank to reject the additional thermal load. Radiator banks comprising of twelve oil filled plates were chosen based on availability from the transformer manufacturer.

4.3 General Problem Statement

This chapter considers a thermosiphon that is incorporated into a 1 MVA transformer as illustrated in Figure 12. Buoyant forces drive oil up through the thermosiphon and the around the coils in the transformer tank and then down through the radiators.

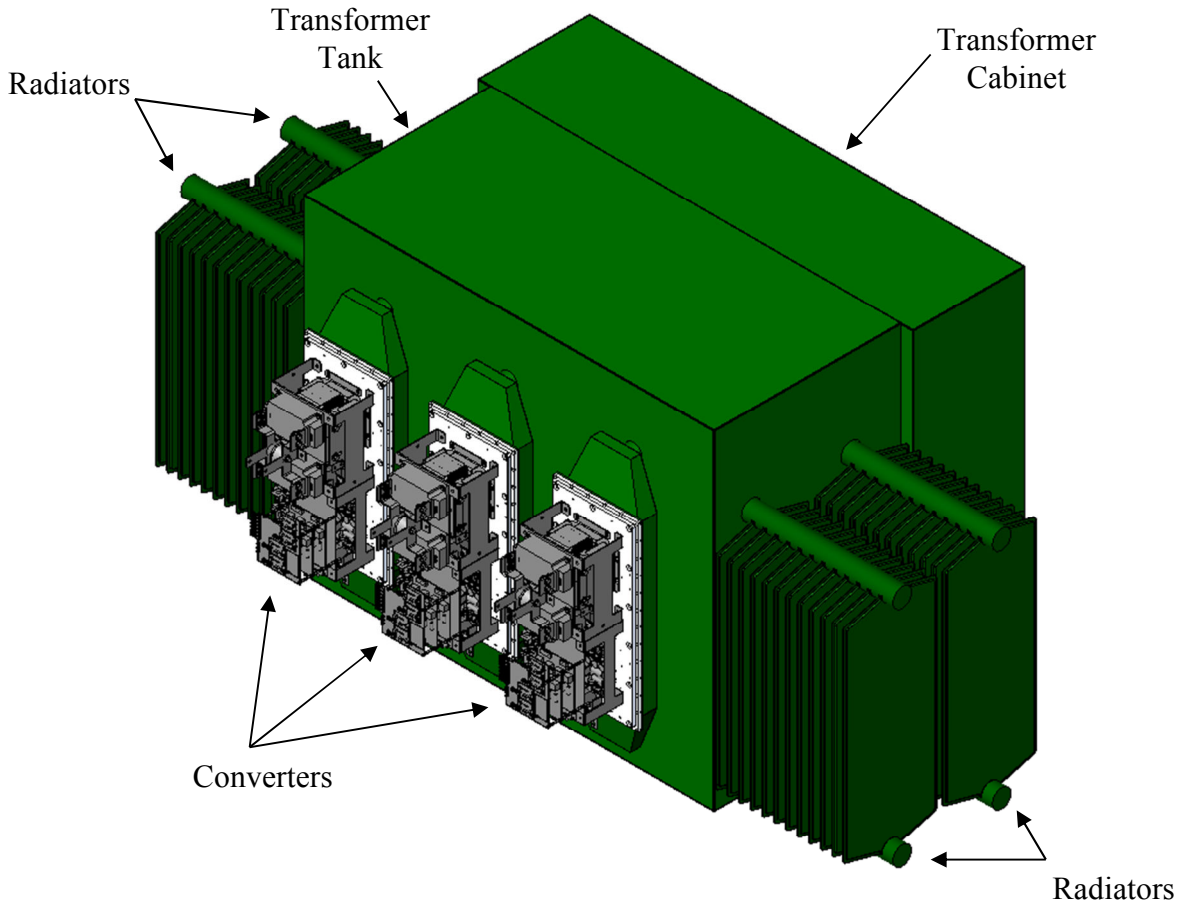

Figure 40. A solid model of the final 1 MVA transformer-thermosiphon assembly

Heat will enter the system from the three converters, each mounted to a baseplate, and from the transformer core located in the center of the transformer tank. A fin array fixed to the baseplate increases the surface area for cooling and allows more heat to be dissipated from the converter. Heat will be rejected through the four radiators located on

the sides of the tank. The transformer consists of the tank, the core, and the coils. The thermosiphon, illustrated in Figure 41, consists of the upper and lower manifolds, the plenum, the fin array which is directly behind the mounting plate, the mounting plate, and the power converter which is not depicted but will be mounted to the mounting plate.

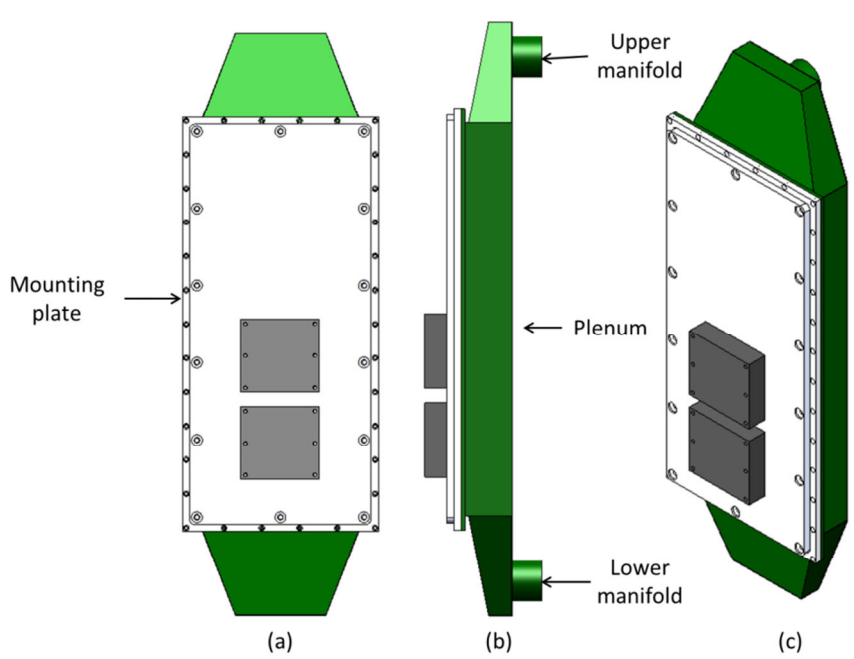

Figure 41. CAD model of the 1 MVA thermosiphon (a) front view, (b) side view and (c) isometric view

The 1 MVA thermosiphon-transformer assembly will be simplified by considering one third of the assembly. It is assumed that the radiators equally dissipate the thermal load. The geometry will again consider three heat transfer planes: transformer heat input, converter heat input and combined ambient rejection. The key specifications for the system are compiled in Table 18.

Table 18. Key design specifications for 1 MVA unit

Description	Metric
Maximum total loss through all converters	2.1 kW
Maximum Total Loss through Transformer	12.388 kW
Maximum $T_{junction}$	125 °C
Maximum $T_{baseplate}$	104.6 °C
Maximum T_{amb}	40 °C
Location for Operation	Southeast

The model is developed so that geometric parameters and heating loads can be varied, solving for the steady state operation in less than 0.1 seconds with an AMD Phenom 9600B Quad-Core Processor 2.30 GHz.

4.4 Analytical Model Modifications

The fluid model circuit used to describe the flow in the 50 kVA assembly was modified, as illustrated in Figure 42, for the 1 MVA assembly.

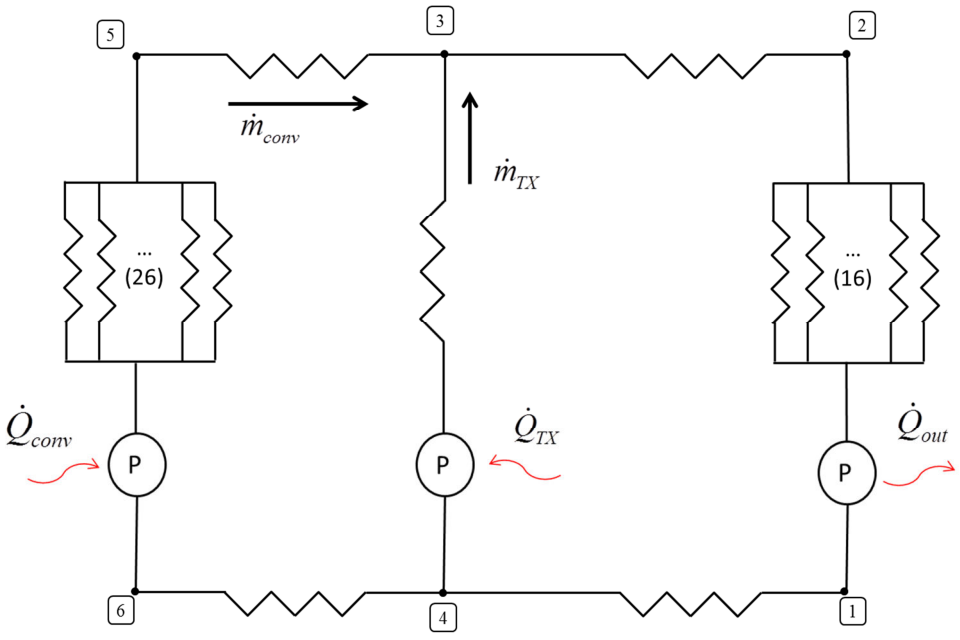

Figure 42: Fluid circuit for the 1 MVA thermosiphon assembly

Location 1 is the bottom of the radiator. Location 6 and 4 are the bottom of the lower manifold and bottom of the transformer core, respectively. The temperature at these locations is considered the same as location 1. Location 2 is the top of the radiator, location 3 is the top of the transformer core and location 5 is the top of the upper manifold. The resistors in Figure 42 represent the pressure losses and the buoyancy gains are represented by the circles. The figure illustrates the flow of the fluid up through both the converter and transformer core and down through the radiator. Mesh analysis along with thermodynamic principles are used to solve the mass flow rates and the temperatures throughout the system. In this analysis, Kirchoff's Law is utilized to ensure that the two pressure loops are balanced.

The pressure loss and buoyancy gain equations utilized in the 50 kVA model remain true in the 1 MVA model. The geometric parameters such as the fin array length and manifold diameters were changed for the geometry of the specific 1 MVA thermosiphon-transformer assembly. Kays formula for expansion and contraction into and out of multiple channels was used for the loss coefficients associated with entering and exiting the radiator. There is also an additional 90° flow change associated with entering and exiting the each radiator plate. The plenum for the converter section also has a geometry change in the 1 MVA configuration. There is a gradual contraction and expansion to a single pipe for the manifold instead of two pipes with no preliminary contraction or expansion.

Additional heat transfer equations were also added to the model to account for the heat dissipated by the radiators. Equation 32 shows Incropera and DeWitt's equation for

heat transfer for free convection between vertical parallel isothermal plates where C_1 and C_2 are 576 and 2.87 respectively and S is the distance between the plates [63].

$$Nu_{radiator} = \left[\frac{C_1}{\left(Ra_s S / L\right)^2} + \frac{C_2}{\left(Ra_s S / L\right)^2} \right]^{-1/2} \quad (32)$$

The incoming insolation was not considered in this model since the effects of surface coating on the incoming radiation were shown in the previous model and the experimental tests would not include a radiative load.

The constraint equations to solve the 1 MVA model were slightly varied to account for the configuration changes and are tabulated in Table 19.

Table 19. Modified constraint equations for 1 MVA thermosiphon-transformer assembly

Constraint equations	Number
$dP_{buoy,conv} - dP_{maj,conv} - dP_{\min,conv} + dP_{buoy,TX} - dP_{maj,TX} = 0$	(1)
$dP_{buoy,CTX} - dP_{maj,CTX} - dP_{\min,CTX} + dP_{buoy,TX} - dP_{maj,TX} = 0$	(2)
$\dot{m}_{conv} \cdot c_p \cdot \left(T_5 - T_2\right) + \dot{m}_{TX} \cdot c_p \cdot \left(T_3 - T_2\right) = 0$	(3)
$Q_c - \dot{m}_{conv} \cdot c_p \cdot \left(T_5 - T_1\right) = 0$	(4)
$Q_{TX} - \dot{m}_{TX} \cdot c_p \cdot \left(T_3 - T_1\right) = 0$	(5)
$Q_c + Q_{TX} + Q_{rad,in} - Q_{conv,out} - Q_{rad,out} = 0$	(6)
$Q_c - \frac{T_{baseplate} - T_{fluid}}{R_{tot}} = 0$	(7)

The analytical model was again implemented in EES v. 9.452 and solved for the steady state temperatures in 0.4 seconds. At maximum transformer and converter load the steady state baseplate temperature is calculated to be 95.95 °C.

4.5 1 MVA thermosiphon construction

The mounting plates were manufactured in MayorLab on a 3-axis CNC mill (Prototrak DPM SX2). Holes for the mounting the plate to the plenum and the fin array to the plate were drilled and the o-ring gasket was machined. The fin array was cut to length and holes were drilled for mounting the fin array to the mounting plate. The fin array was fixed to the mounting plate with Duralco 132, a thermally conductive aluminum epoxy, in addition to 9 8/32 bolts. Once the mounting plates were assembled with the fin arrays and O-rings, depicted in they were shipped to T&R Electric. The plenums for each thermosiphon were constructed by T&R where the mounting plates were then attached to the assembly. Each individual thermosiphon was then welded onto the 1 MVA transformer before being shipped back to NEETRAC for testing.

Figure 43. Assembled mounting plates for 1 MVA thermosiphon

4.6 1 MVA thermosiphon-transformer testing

The 1 MVA thermosiphon-transformer assembly was required to be tested at an ambient temperature of 40 °C. The size and additional thermal load in the 1 MVA assembly required a larger thermal chamber than the 50 kVA testing. A 16’ x 16’ chamber was designed and then built at NEETRAC to perform the elevated ambient testing. The 16’x16’ chamber was built from 2”x4” frame with foam insulation board filling the gaps to reduce heat loss through the walls. A viewing window constructed of plexi-glass allows for early detection of any problems during the testing. Half of the chamber from the 50kVA testing was incorporated into one of the walls to provide the inlet air flow. Four DC fans, built into one of the chamber walls, were utilized for flow rate control through the chamber. A wall of honeycomb, located between the test section and the fans, created laminar air flow into the test section. Insulation board was used to cover the concrete floor of the test section because the concrete acts as a heat sink making the elevated temperature increasingly difficult to maintain without the insulation. A digital proportional-derivative-integral (PID) control was used to the control the voltage to the fans and therefore the temperature within the chamber. Four T-type thermocouples were used to measure the ambient temperature within the chamber, which were the input to the PID controller. The PID controller calculates the error as the difference between the measured ambient temperature and the desired set point temperature. The PID controller utilizes the values for the proportional, derivative and integral gain to adjust the output, in this case the voltage to the fans, to minimize this error. The necessary mass flow into the chamber was calculated using Equation (33). This mass flow rate was used to determine the number of fans that would be needed.

$$\dot{m} = \frac{\dot{Q}_{loss} - \dot{Q}_{walls} - \dot{Q}_{floor}}{c_p \left(T_{chamber} - T_{\infty} \right)} \qquad (33)$$

The mass flow rate was calculated with varying insulation thickness and varying external ambient temperatures as shown in Figure 44.

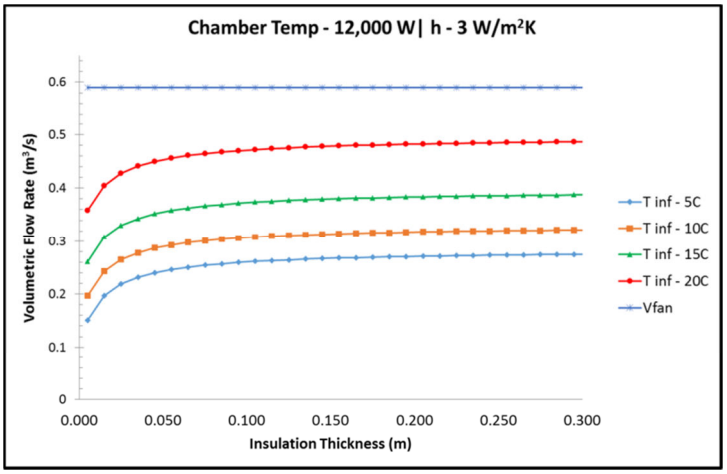

Figure 44. Volumetric flow rate needed to dissipate 12 kW of heat with various insulation thickness and external ambient temperatures

The CAD model for the final thermal chamber design is depicted in Figure 45.

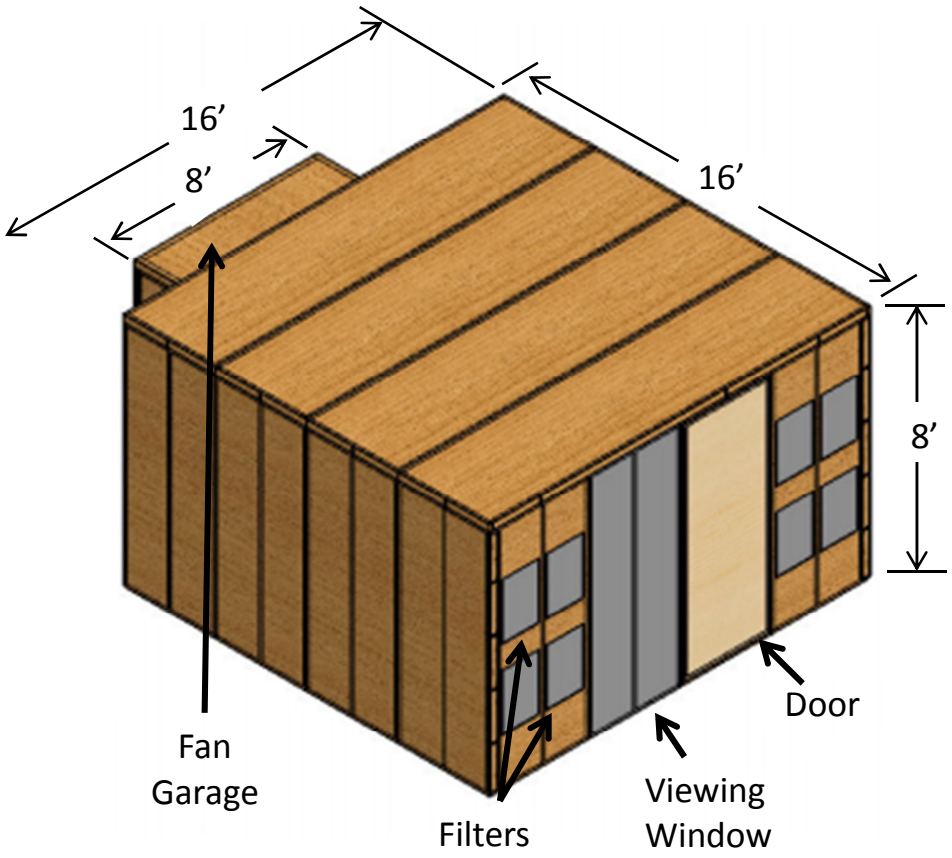

Figure 45. Final thermal chamber design

The baseplate temperatures, as shown schematically in Figure 46, were measured at two points on all three baseplates: at the bottom and at the top. Having the top and bottom plate temperatures confirmed that the thermosiphons were cooling the converters rather than acting as additional radiators. Measuring across all three plates gave insight into whether each thermosiphon was receiving equal oil flow and cooling power. The top and bottom manifold temperature of one of the radiators was measured to give insight into the effectiveness of the radiators. All temperatures were measured with surface thermocouples and recorded using a 16-channel DAQ card, NI 9213.

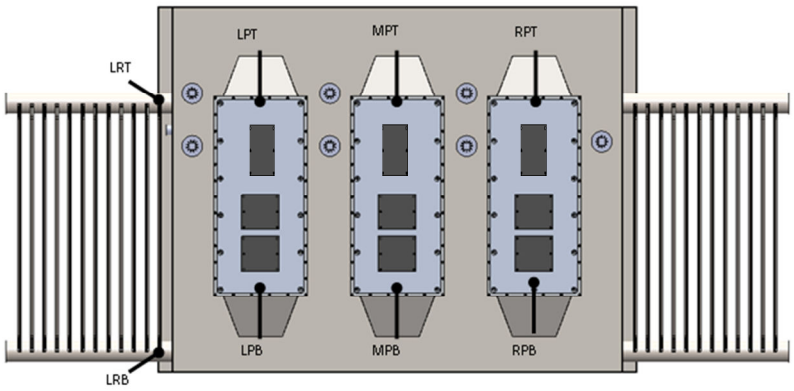

Figure 46. Schematic of thermocouple locations

The same measurement equipment used for the 50 kVA testing was again used for the 1 MVA, given again in Table 20 for reference.

Table 20: Apparatus with associated uncertainty

Measurement Apparatus	Model	Uncertainty
Digital Voltmeter	Fluke 179	1.0% + 3 counts
Digital Ohmmeter	Fluke 179	0.9% + 1 count
Surface Thermocouple	Omega T-type	1.0 °C
Thermocouple	Omega T-type	1.0 °C
Variac	Staco 3PN1010	N/A
16 Ch. Thermocouple DAQ	NI 9213	N/A

The 1 MVA GCD-PAR in the thermal chamber prior to testing is illustrated in Figure 47.

Figure 47: GCD-PAR thermosiphon-transformer assembly in the thermal chamber prior to testing

A full 12 hour at test was performed with the results from the test are displayed in Figure 48.

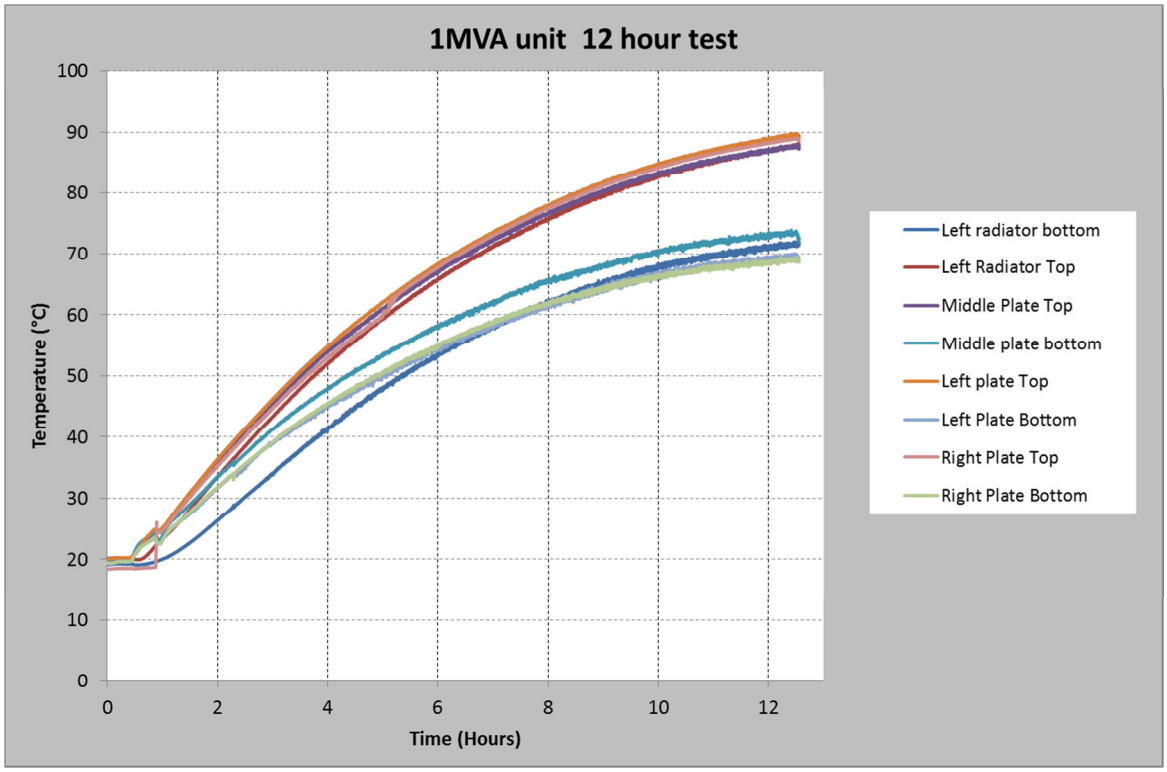

Figure 48: 1 MVA 12 Hour thermosiphon-transformer testing results

The data shows that the cold plates never breached the critical temperature of 104.6°C during the test. The temperatures did not reach steady state during the testing although the temperatures appeared to be stabilizing. The temperatures approaching steady state is illustrated by the dT/dt graphs shown below in Figure 49. The graphs show the change in temperature over the change in time. Once the line reaches zero, the system has effectively reached steady state as the temperature is no longer changing with respect to time. The plots were created from the temperature data of the cold plates and radiators. The dT/dt lines approach but never cross the X axis, meaning the system never reached steady state.

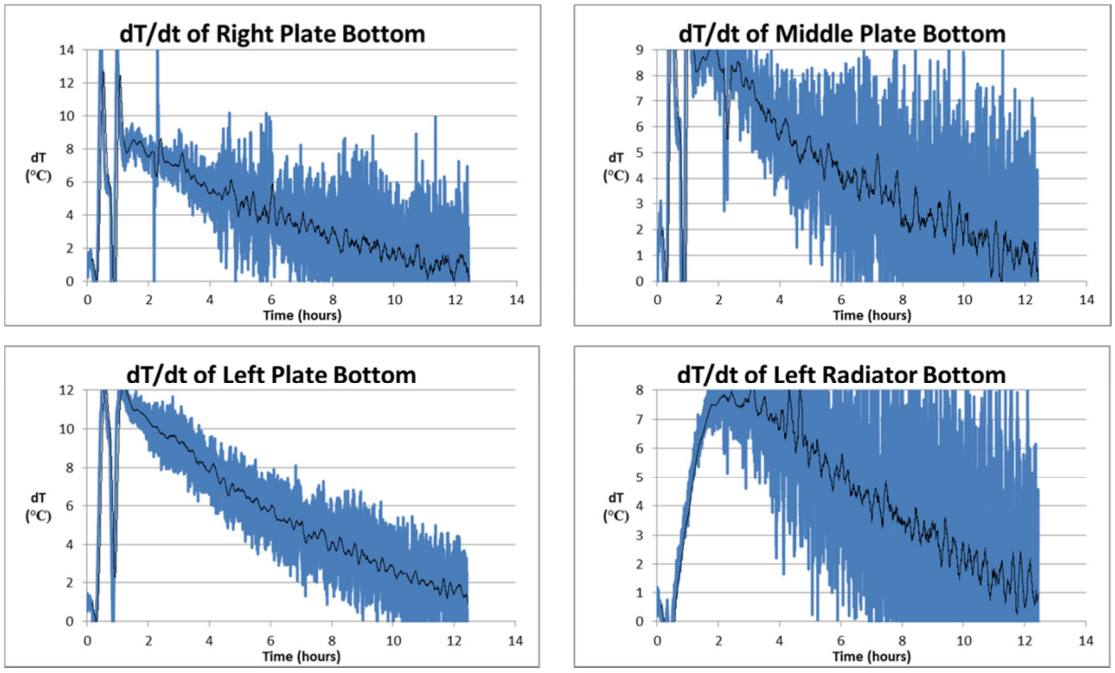

Figure 49: The dT/dt plots of the 1 MVA test results

The length of the test was limited to 12 hours at NEETRAC to comply with safety regulations. The temperature data was extrapolated using the same method that was

utilized for the 50 kVA assembly testing temperatures. The final temperatures after the 12 hour test, along with the extrapolated temperatures are tabulated in Table 21.

Table 21: 1 MVA 12 hour testing temperatures and extrapolated steady state temperatures

Thermocouple Location	Temperature after 12 hours [°C]	Extrapolated steady state temperatures [°C]
Left Plate Top	89.18	93.38
Left Plate Bottom	69.19	73.34
Middle Plate Top	87.3	91.53
Middle Plate Bottom	72.55	76.6
Right Plate Top	88.61	92.85
Right Plate Bottom	68.64	72.86
Radiator Top	87.8	92.01
Radiator Bottom	71.49	75.76

From the extrapolated steady state temperatures, the maximum differential between the top mounting plate temperatures is 1.85 °C. With an uncertainty of ±1°C associated with each thermocouple reading, a 2° difference could be associated to the uncertainty. With that, it is a reasonable assumption to state that the three mounting plates receive equal cooling from the respective thermosiphons. The bottom temperatures are also significantly lower than the top plate temperatures showing that the flow is operating in the correct direction and the thermosiphons are not acting as additional radiators heating up the converters. The steady state top plate temperatures described by the curve fits were compared to the steady state plate temperature given by the analytical model as tabulated in Table 22.

Table 22: Analytical EES steady state temperatures compared to experimental steady state temperatures

Description	Experimental [°C]	Model Prediction [°C]	Difference [°C]
Left Plate	93.38	95.5	2.12
Middle Plate	91.53		3.97
Right Plate	92.85		2.65

The maximum difference between the experimental measurements and model prediction was the middle mounting plate temperature at 3.97 °C.

4.7 Summary

An analytic thermo-fluidic model for a 1 MVA dual-loop single phase thermosiphon-transformer assembly is presented. The thermosiphon-transformer assembly is constructed and tested experimentally at an ambient temperature of 40 °C to compare experimental results to the model results. The maximum disagreement between the model and experimental data was 3.97 °C for the mounting plate temperatures. The code solves in less than 0.4 seconds and accurately predicts the performance of a given thermosiphon-transformer assembly.

CHAPTER 5

CONCLUSTION

5.1 Summary and conclusions

This work provides a viable solution for the thermal management of high power electronics coupled to various distribution grid assets. The GCD-PAR presents a unique problem where the electronics needing to be cooled passively are located near a transformer full of oil. Thermosiphons were incorporated into a grounded compact dynamic phase angle regulator (GCD-PAR) that aimed to facilitate power routing and reduce line losses on the power grid. The power router utilizes power electronics that reject heat to a planar area, or cold plate, which must be cooled by an entirely passive system to comply with the minimum 30 year mean time between failures (MTBF) consistent with grid reliability requirements. This design includes a secondary-loop cooling path that utilizes the cooling oil already present in the transformer to also cool the power router. An analytical thermosiphon model was developed that couples existing fluid dynamic and heat transfer correlations to create a description of the steady state operation of a specific cylindrical 50 kVA transformer augmented with a thermosiphon. The analytical model was again implemented in EES v. 9.452 and solved for the steady state temperatures in 0.1 seconds. The model was validated experimentally at two different ambient conditions and found to solve for steady state baseplate temperatures under maximum load within 2 °C and the thermal resistance within 2.5% error in 0.1 seconds. A similar thermosiphon-transformer assembly is then designed for a three-phase 13 kV transformer with up to 1 MVA of power flow control. The analytical model is then modified for the final rectilinear 1 MVA transformer design augmented with three

thermosiphons. The 1 MVA model is validated experimentally at maximum ambient conditions and thermal load and found to solve for steady state baseplate temperatures under maximum load within 4 °C in 0.2 seconds. The accuracy of the model decreases in accuracy and increases in time to solve to the increased complexity and additional cooling path presented in the 1 MVA thermosiphon configuration. The analytical model proves to be accurate and solve quickly with various geometric configurations and thermal loads. This shows the applicability of the analytical model to various configurations, and by modifying the pressure loss coefficients, geometric parameters and thermal loads that the analytical model can be used to describe the steady state operation of almost any dual-loop single phase thermosiphon system with two heat inputs and one cooling path.

Pursuant to work summarized here and presented in the previous chapters, the following conclusions can be made:

- An analytical thermo-fluidic single-phase dual loop transformer-thermosiphon model was developed for a 1 MVA and 50 kVA transformer both augmented with thermosiphons for passive cooling of power electronics.
- The analytical thermo-fluidic single-phase dual loop transformer-thermosiphon model for the 50 kVA assembly with 780 W of total heat input predicted mounting plate temperature within 2 °C and thermosiphon thermal resistance within 2.5%.
- The analytical thermo-fluidic single-phase dual loop transformer-thermosiphon model for the 1 MVA assembly with 780 W of total heat input predicted mounting plate temperature within 4 °C.

- The analytical thermo-fluidic single-phase dual loop transformer-thermosiphon models quickly and accurately predicted steady state mounting plate temperatures at two different geometric configurations and thermal loads showing its possible applicability to other similar dual-loop thermosiphon systems.

5.2 Contributions

Pursuant the work summarized above and presented in the previous chapters, the following contributions were made:

- A unique design was created to passively cool power electronics by augmenting transformers with single phase thermosiphons to use the existing transformer oil to also cool the power electronics.
- A thermo-fluidic analytical model was developed and experimentally verified for a both a 50 kVA and 1 MVA thermosiphon –transformer assembly.
- An analytical model was developed to accept geometric parameters and thermal loads as inputs to solve for the steady state operation of dual-loop single phase thermosiphons.
- The following paper has been published:

  Danielle Hesse, J. Rhett Mayor, S. Andrew Semidey (2014). Analytical Modeling of Dual-Loop Single Phase Thermosiphons for Power Electronics Cooling. ASME 2014 International Mechanical Engineering Congress and Exposition. Montreal, Quebec, Canada. **8A: Heat Transfer and Thermal Engineering:** 8.

5.3 Recommendations and future work

During the course of this study, several possible extensions of this work were identified. These extensions are presented here as recommendations for future work.

- Create a rapid design sizing tool from the analytical model

A rapid passive thermal management design sizing tool can be created by implementing the thermo-fluidic model in a numerical optimization. A particle swarm optimization or genetic algorithm can be utilized to define the optimal geometric parameters for various dual-loop thermosiphon configurations.

- Hot side feature enhancement

It is known that by reducing the thermal resistance from a heating device to the heat transfer fluid, more heat can be dissipated into the heat transfer fluid and the critical junction temperature can be reduced. It was also seen in this work that the contraction and expansion into and out of the fin array accounted for over 75% of the pressure loss in the converter section. Decreasing this pressure loss would increase the mass flow rate through the converter section and also increase heat transfer from the power electronics to the heat transfer fluid. Exploration should be done to find the optimal heat sink geometry for the given application. Studs, specifically of the hydrofoil shape, offer increased heat transfer with a decrease in pressure drop. Utilizing this technology would have the possibility of increased thermosiphon and system performance.

REFERENCES

[1] "State Electricity Profiles - Data for 2012," U. S. E. I. Administration, Ed., ed, 2014.

[2] M. B. Jacobs, "Transmission Recommendations for High Wind Penetration," *IEEE Power Engineering Society General Meeting,* 2007.

[3] Available: http://www.hitachi.com/environment/showcase/solution/energy/smartgrid.html

[4] Infineon. (2015). *INFINEON FZ1000R33HE3 IGBT, HI PO, 1 S/W, 3300V, 1000A*. Available: http://uk.farnell.com/infineon/fz1000r33he3/igbt-hi-po-1-s-w-3300v-1000a/dp/1833605

[5] A. Prasai, R. P. Kandula, and D. Divan, "Design Considerations and Experimental Results for a 13-kV 3-Phase 1 MVA Power Router," presented at the ECCE, 2015.

[6] (2012). *Insulation System Thermal Life Expectancy vs Total Operating Temperature*. Available: www.marathonelectric.com/generators/docs/manuals/thermal-life.pdf

[7] Y. F. Mayadanik, "Loop Heat Pipes," *Applied Thermal Engineering,* vol. 25, pp. 635-657, 2005.

[8] B. H. Loeffler, "Modeling and Optimization of a Thermosiphon for Passive Thermal Management Systems," Master of Science, G.W. Woodruff School of Mechanical Engineering, Georgia Institute of Technology, 2012.

[9] S. a. S. Arneth, J., "Characteristics of thermosyphon reboilers," *International Journal of Thermal Sciences,* vol. 40, pp. 385-391, 2001.

[10] K. C. Cheng, Morioka I.,Ichimiya K., Sadler G.W., "Experimental study of a two-phase thermosyphon system," *Alternative Energy Sources,* vol. 1, pp. 151-170, 1982.

[11] V. K. a. B. Chexal, A.E., "Two-phase instabilities in a low pressure natural circulation loop," *AIChE Symposium Series,* vol. 69, pp. 37-45, 1982.

[12] R. T. a. R. Dobson, J.C., "Flow and Heat Transfer in a Closed loop thermosyphon Part I - Theoretical simulation," *Journal of Energy Southern Africa,* vol. 18, pp. 32-40, 2007.

[13] R. a. P. Khodabandeg, B., "Influence of system pressure on the boiling heat transfer coefficient in a closed two-phase thermosyphon loop," *International Journal of Thermal Sciences,* vol. 41, pp. 619-624, 2002.

[14] T. Yilmaz, "Computer simulation of two-phase flow thermosyphon solar water heating system," *Energy Convers. Mgmt.,* vol. 32, pp. 133-144, 1991.

[15] P. Welander, *Fluid Mechanics,* vol. 29, pp. 17-30, 1967.

[16] en:User:Glogger. *Polemount-singlephase-closeup*. Available: http://commons.wikimedia.org/wiki/File:Polemount-singlephase-closeup.jpg#/media/File:Polemount-singlephase-closeup.jpg

[1] "State Electricity Profiles - Data for 2012," U. S. E. I. Administration, Ed., ed, 2014.

[2] M. B. Jacobs, "Transmission Recommendations for High Wind Penetration," *IEEE Power Engineering Society General Meeting,* 2007.

[3] Available: http://www.hitachi.com/environment/showcase/solution/energy/smartgrid.html

[4] Infineon. (2015). *INFINEON FZ1000R33HE3 IGBT, HI PO, 1 S/W, 3300V, 1000A*. Available: http://uk.farnell.com/infineon/fz1000r33he3/igbt-hi-po-1-s-w-3300v-1000a/dp/1833605

[5] A. Prasai, R. P. Kandula, and D. Divan, "Design Considerations and Experimental Results for a 13-kV 3-Phase 1 MVA Power Router," presented at the ECCE, 2015.

[6] (2012). *Insulation System Thermal Life Expectancy vs Total Operating Temperature*. Available: www.marathonelectric.com/generators/docs/manuals/thermal-life.pdf

[7] T. Fisher and K. Torrance, "Free Convection Limits for Pin-fin Cooling," *Journal of Heat Transfer,* vol. 120, p. 633, 1998.

[8] Y. F. Mayadanik, "Loop Heat Pipes," *Applied Thermal Engineering,* vol. 25, pp. 635-657, 2005.

[9] B. H. Loeffler, "Modeling and Optimization of a Thermosiphon for Passive Thermal Management Systems," Master of Science, G.W. Woodruff School of Mechanical Engineering, Georgia Institute of Technology, 2012.

[10] S. a. S. Arneth, J., "Characteristics of thermosyphon reboilers," *International Journal of Thermal Sciences,* vol. 40, pp. 385-391, 2001.

[11] K. C. Cheng, Morioka I.,Ichimiya K., Sadler G.W., "Experimental study of a two-phase thermosyphon system," *Alternative Energy Sources,* vol. 1, pp. 151-170, 1982.

[12] V. K. a. B. Chexal, A.E., "Two-phase instabilities in a low pressure natural circulation loop," *AIChE Symposium Series,* vol. 69, pp. 37-45, 1982.

[13] R. T. a. R. Dobson, J.C., "Flow and Heat Transfer in a Closed loop thermosyphon Part I - Theoretical simulation," *Journal of Energy Southern Africa,* vol. 18, pp. 32-40, 2007.

[14] R. a. P. Khodabandeg, B., "Influence of system pressure on the boiling heat transfer coefficient in a closed two-phase thermosyphon loop," *International Journal of Thermal Sciences,* vol. 41, pp. 619-624, 2002.

[15] T. Yilmaz, "Computer simulation of two-phase flow thermosyphon solar water heating system," *Energy Convers. Mgmt.,* vol. 32, pp. 133-144, 1991.
[16] P. Welander, *Fluid Mechanics,* vol. 29, pp. 17-30, 1967.
[17] en:User:Glogger. *Polemount-singlephase-closeup*. Available: http://commons.wikimedia.org/wiki/File:Polemount-singlephase-closeup.jpg#/media/File:Polemount-singlephase-closeup.jpg
[18] D. J. a. E. R. F. Winter, "Single-phase transport processes in the open thermosyphon," *Journal of Heat and Mass Transfer,* vol. 14, pp. 427-441, 1971.
[19] E. R. a. C. T. Mihir Sen, "The toroidal thermosyphon with known heat flux," *International Journal of Heat and Mass Transfer,* vol. 28, pp. 219-233, 1985.
[20] J. F. d. P. H. F. Creveling, J. Y. Baladi and R. J. Schoenhals, "Stability characteristics of a single-phase free convection loop," *Journal of Fluid Mechanics,* vol. 67, pp. 65-84, 1975.
[21] Y. Z. a. A. M. R. Greif, "The transient and stability behavior of a natural circulation loop," *Journal of Heat Transfer,* vol. 101, pp. 684-688, 1979.
[22] P. S. D. a. R. J. Schoenhals, "Flow in a toroidal thermosyphon with angular displacement of heated and cooled sections," *Journal of Heat Transfer,* vol. 101, pp. 672-675, 1979.
[23] J. E. Hart, "A new analysis of the closed loop thermosyphon," *International Journal of Heat and Mass Transfer,* vol. 27, pp. 125-136, 1984.
[24] Y. Zvirin, "A Review of Natural Circulation Loops in PWR and Other Systems," *Nuclear Engineering Design,* vol. 67, pp. 203-225, 1981.
[25] A. Mertol and R. Greif, "REVIEW OF NATURAL CIRCULATION LOOPS," in *Natural Convection: Fundamentals and Applications.*, Washington, DC, USA, 1985, pp. 1033-1071.
[26] T. F. I. Ishihara, and R. Matsumoto, "Natural convection in a vertical rectangular enclosurewith symmetrically localized heating and cooling zones 1," *International Journal of Heat and Fluid Flow,* vol. 23, pp. 366-372, 2002.
[27] K. Nakagawa and I. Ishihara, "Flow characteristics in a single phase closed thermosyphon," *Nippon Kikai Gakkai Ronbunshu, B Hen/Transactions of the Japan Society of Mechanical Engineers, Part B,* vol. 70, pp. 2349-2354, 2004.
[28] M. Maiani, W. d. Kruijf, and W. Ambrosini, "An analytical model for the determination of stability boundaries in a natural circulation single-phase thermosyphon loop," *International Journal of Heat and Fluid Flow,* vol. 24, pp. 853-863, 2003.
[29] E. Burroughs, E. Coutsias, and L. Romero, "A reduced-order partial differential equation model for the flow in a thermosyphon," *Journal of Fluid Mechanics,* vol. 543, pp. 203-237, 2005.
[30] P. K. Vijayan, "Experimental observations on the general trends of the steady state and stability behavior of single-phase natural circulation loops," *Nuclear Engineering and Design,* vol. 215, pp. 139-152, 2002.
[31] M. R. G. P.K. Vijayan, D.S. Pilkhwal, G.S.S.P. Rao and D. Saha, "Steady State Behaviour of Single-Phase and Two-Phase Natural Circulation Loops," *RCM of the IAEA CRP,* vol. 2, 2005.
[32] D. C. Hamilton and L. D. Palmer, "The Nature of the Flow of Ordinary Fluids in a Thermal Convection Harp," O. R. N. Laboratory, Ed., ed, 1954.

[33] D. Close, "The performance of solar water heaters with natural circulation," *Solar Energy,* vol. 6, pp. 33-40, 1962.
[34] K. Ong, "A finite-difference method to evaluate the thermal performance of a solar water heater," *Solar Energy,* vol. 16, pp. 137-147, 1974.
[35] K. Ong, "An improved computer program for the thermal performance of a solar water heater," *Solar Energy,* vol. 18, pp. 183-191, 1976.
[36] M. Bernier and B. Baliga, "A 1-D/2-D model and experimental results for a closed-loop thermosyphon with vertical heat transfer sections," *International Journal of Heat and Mass Transfer,* vol. 35, 1992.
[37] M. Poplentini, S. Ramadhyani, and F. Incropera, "Single-phase thermosyphon cooling of an array of discrete heat sources in a rectangular cavity," *International Journal of Heat and Mass Transfer,* vol. 36, pp. 3983-3996, 1993.
[38] H. B. a. J. Mikielewicz, " Natural Circulation in Single and Two Phase Thermosyphon Loop with Conventional Tubes and Minichannels," in *Heat Transfer - Mathematical Modelling, Numerical Methods and Information Technology*, P. A. Belmiloud, Ed., ed: InTech, 2011.
[39] P. I. Rosen Esquivel, J. H. M. ten Thije Boonkkamp, J. A. M. Dam, and M. M. Mattheij, "Wall shape optimization for a thermosyphon loop featuring corrugated pipes," in *Advances in Cryogenic Engineering: Cryogenic Engineering Conference - CEC, 13-17 June 2011*, USA, 2012, pp. 724-31.
[40] R. T. a. R. Dobson, J.C., "Flow and Heat Transfer in a Closed loop thermosyphon Part II - Experimental simulation," *Journal of Energy Southern Africa,* vol. 18, pp. 32-40, 2007.
[41] B. H. Loeffler, "MODELING AND OPTIMIZATION OF A THERMOSIPHON FOR PASSIVE THERMAL MANAGEMENT SYSTEMS," Master of Science in Mechanical Engineering, Mechanical Engineering, Georgia Institute of Technology, 2012.
[42] I. Standards, "IEEE Guide for Loading Mineral-Oil-Immersed Transformers," ed, 1996.
[43] L. W. Pierce, "Predicting liquid filled transformer loading capability," *Industry Applications, IEEE Transactions on* vol. 30, pp. 170-178, 1994.
[44] A. J. Oliver, "Estimation of transformer winding temperatures and coolant flows using a general network method," *Generation, Transmission and Distribution, IEE Proceedings C,* vol. 127, pp. 395-405, 1980.
[45] R. M. D. Vecchio, *Transformer Design Principles: With Applications to Core-Form Power Transformers*, 2001.
[46] G. Swift, T. S. Molinski, and W. Lehn, "A fundamental approach to transformer thermal modeling. I. Theory and equivalent circuit," *IEEE Transactions on Power Delivery,* vol. 127, pp. 395-405, 2001.
[47] G. Swift, T. S. Molinski, R. Bray, and R. Menzies, "A fundamental approach to transformer thermal modeling. II. Field verification," *IEEE Transactions on Power Delivery,* vol. 16, pp. 176-180, 2004.
[48] T. Shintomi, T. Asami, G. Suzuki, N. Ota, T. Takao, Y. Makida*, et al.*, "Design study of MgB2 SMES coil for effective use of renewable energy," *IEEE Transactions on Applied Superconductivity,* vol. 23, 2013.

[49] R. Sacco, L. Carichino, C. de Falco, M. Verri, F. Agostini, and T. Gradinger, "A multiscale thermo-fluid computational model for a two-phase cooling system," *Computer Methods in Applied Mechanics and Engineering,* vol. 282, pp. 239-68, 12/01 2014.
[50] M. Merio, M. J. Lamm, A. Martinez, T. M. Page, and T. J. Peterson, "Preliminary design of the production solenoid feedbox for the mu2e project at fermilab," *IEEE Transactions on Applied Superconductivity,* vol. 25, 2015.
[51] T. B. Gradinger and F. Agostini, "Assessment of Two-Phase Cooling of Power Electronics Using Roll-Bonded Condensers," *Journal of Thermal Science and Engineering Applications,* vol. 7, 2014.
[52] M. S. Gandhi, J. B. Joshi, and P. K. Vijayan, "Study of two phase thermal stratification in cylindrical vessels: CFD simulations and PIV measurements," *Chemical Engineering Science,* vol. 98, pp. 125-151, 2013.
[53] E. Aguayo, J. E. Fast, and D. J. Reid, "Design of a thermosiphon for cooling low-background HPGe arrays," in *Advances in Cryogenic Engineering: Cryogenic Engineering Conference - CEC, 13-17 June 2011*, USA, 2012, pp. 425-32.
[54] D. Liu, F.-Y. Zhao, H.-X. Yang, and G.-F. Tang, "Thermoelectric mini cooler coupled with micro thermosiphon for CPU cooling system," *Energy,* vol. 83, pp. 29-36, 2015.
[55] S. S. Kang, "Advanced cooling for power electronics," in *2012 7th International Conference on Integrated Power Electronics Systems, CIPS 2012, March 6, 2012 - March 8, 2012*, Nuremberg, Germany, 2012.
[56] M. Y. Okiishi, *Fundamentals of Fluid Mechanics*, Fifth ed.: John Wiley & Sons, 2006.
[57] W. M. Kays, "Loss coefficients for abrupt changes in flow cross section with low Reynolds number flow in single and multiple-tube systems," *American Society of Mechanical Engineers -- Transactions,* vol. 72, pp. 1067-1074, 1950.
[58] I. E. Idel'chik, *Handbook of Hydraulic Resistance*, 3 ed.: Begell House, 1996.
[59] A. S. D. Center. NASA Surface meteorolog and Solar Energy [Online].
[60] I. D. B. Lavine, *Fundamentals of Heat and Mass Transfer*, Sixth ed.: John Wiley & Sons, Inc., 2007.
[61] U. S. D. o. t. Interior, "Facilities Instruction, Standard, and Techniques," in *Painting of Transformers and Circuit Breakeres*, ed, 1991.
[62] M. R. Warren, J. P. Hartnett, and Y. I. Cho, *Handbook of Heat Transfer*, 3rd ed.: McGraw-Hill, 1998.
[63] F. P. Incropera and D. P. DeWitt, *Introduction to Heat Transfer*, 3rd ed., 1996.